Redox Biology 74 (2024) 103202

Contents lists available at ScienceDirect

Redox Biology

journal homepage: www.elsevier.com/locate/redox

Development of nitroalkene-based inhibitors to target STING-dependent inflammation

Fei Chang [a], Camilla Gunderstofte [b], Nicole Colussi [a], Mareena Pitts [c], Sonia R. Salvatore [a], Anne L. Thielke [b], Lucia Turell [d,e], Beatriz Alvarez [d,e], Raphaela Goldbach-Mansky [f], Luis Villacorta [c,****], Christian K. Holm [b,**], Francisco J. Schopfer [a,g,h,i,***], Anne Louise Hansen [b,*]

[a] Department of Pharmacology and Chemical Biology, University of Pittsburgh, Pittsburgh, PA, 15213, USA
[b] Department of Biomedicine, Aarhus University, 8000, Aarhus C, Denmark
[c] Department of Physiology, Morehouse School of Medicine, Atlanta, GA, 30310, USA
[d] Laboratorio de Enzimología, Instituto de Química Biológica, Facultad de Ciencias, Universidad de la República, Montevideo, 11400, Uruguay
[e] Centro de Investigaciones Biomédicas (CEINBIO), Universidad de la República, Montevideo, 11800, Uruguay
[f] Translational Autoinflammatory Disease Studies Unit, National Institute of Allergy and Infectious Diseases, NIH, Bethesda, MD, 20850, USA
[g] Pittsburgh Heart, Lung, Blood, And Vascular Medicine Institute (VMI), Pittsburgh, PA, USA
[h] Pittsburgh Liver Research Center (PLRC), Pittsburgh, PA, USA
[i] Center for Metabolism and Mitochondrial Medicine (C3M), Pittsburgh, PA, USA

ARTICLE INFO

Keywords:
Stimulator of Interferon Genes (STING)
Drug discovery
Nitroalkene-based compounds
STING inhibitors
STING-associated vasculopathy with onset in infancy (SAVI)
Interferon

ABSTRACT

Stimulator of Interferon Genes (STING) is essential for the inflammatory response to cytosolic DNA. Despite that aberrant activation of STING is linked to an increasing number of inflammatory diseases, the development of inhibitors has been challenging, with no compounds in the pipeline beyond the preclinical stage. We previously identified endogenous nitrated fatty acids as novel reversible STING inhibitors. With the aim of improving the specificity and efficacy of these compounds, we developed and tested a library of nitroalkene-based compounds for *in vitro* and *in vivo* STING inhibition. The structure-activity relationship study revealed a robustly improved electrophilicity and reduced degrees of freedom of nitroalkenes by conjugation with an aromatic moiety. The lead compounds CP-36 and CP-45, featuring a β-nitrostyrene moiety, potently inhibited STING activity *in vitro* and relieved STING-dependent inflammation *in vivo*. This validates the potential for nitroalkene compounds as drug candidates for STING modulation to treat STING-driven inflammatory diseases, providing new robust leads for preclinical development.

1. Introduction

The cyclic GMP-AMP (cGAMP) synthase (cGAS) is the primary cytosolic sensor of double-stranded DNA (dsDNA) in mammalian cells. Binding of dsDNA to cGAS prompts the synthesis of the second messenger molecule 2′3′-cGAMP (cGAMP) [1–4], a potent activator of the intracellular adaptor molecule Stimulator of Interferon Genes (STING) (also known as MPYS, ERIS, MITA, TMEM173 or STING1). STING activation is an indispensable step for the induction of type I interferons (IFNs, i.e., IFNα and IFNβ) and pro-inflammatory cytokines [5–11].

STING-mediated signaling comprises STING translocation from the endoplasmic reticulum (ER) through the ER-Golgi intermediate compartments (ERGIC) and Golgi to post-Golgi vesicles [12–14]. STING exists as a constitutive dimer but undergoes stabilizing conformational changes upon binding of cGAMP. These changes involve a 180° rotation,

* Corresponding author. Department of Biomedicine, Aarhus University, 8000 Aarhus C, Denmark
** Corresponding author. Department of Biomedicine, Aarhus University, 8000 Aarhus C, Denmark
*** Corresponding author. Department of Pharmacology and Chemical Biology, University of Pittsburgh, Pittsburgh, PA 15213, USA
**** Cooresponding author. Department of Physiology, Morehouse School of Medicine, Atlanta, GA 30310, USA
E-mail addresses: lvillacortaperez@msm.edu (L. Villacorta), holm@biomed.au.dk (C.K. Holm), fjschopfer@katz.pitt.edu (F.J. Schopfer), annelouisehansen@biomed.au.dk (A.L. Hansen).

https://doi.org/10.1016/j.redox.2024.103202
Received 18 April 2024; Received in revised form 18 May 2024; Accepted 19 May 2024
Available online 21 May 2024
2213-2317/© 2024 The Authors. Published by Elsevier B.V. This is an open access article under the CC BY-NC-ND license (http://creativecommons.org/licenses/by-nc-nd/4.0/).

"lid-closing" and the oligomerization of STING dimers [1,15–20]. Additionally, posttranslational modifications such as the indispensable palmitoylation of cysteine residues (i.e., Cys88/91) is required for maximal activation [21]. The C-terminal tail of STING provides a scaffold for the recruitment of the TANK-binding kinase 1 (TBK1) and TBK1 autophosphorylation [22,23] as well as phosphorylation of STING at Ser366 and enhanced binding of interferon regulatory factor 3 (IRF3) [24–26]. The TBK1-promoted phosphorylation of IRF3 allows for IRF3 dimerization and translocation to the nucleus for the final induction of type I IFNs and interferon-stimulated genes (ISGs) [27]. In parallel, STING activation causes NFκB to upregulate several pro-inflammatory mediators [28,29] as well as the induction of autophagy [30].

A slew of autoimmune and inflammatory conditions, including systemic lupus erythematosus (SLE), Aicardi-Goutières syndrome (AGS) and COPA syndrome, are associated with aberrant STING activation and a pathological induction of type I IFNs and ISG signatures [31–33]. Additionally, rare gain-of-function mutations in the STING-encoding gene *TMEM173,* result in ligand-independent STING activation by spontaneous conformational changes and translocation of STING [34]. This STING overactivation causes the severe autoinflammatory syndrome STING-associated vasculopathy with onset in infancy (SAVI) [35]. SAVI patients show a clinical presentation of early-onset systemic inflammation, severe skin vasculopathy, and interstitial lung disease, causing pulmonary fibrosis and respiratory failure [35]. Therapeutic interventions in the reported patient cases have so far proven unsatisfactory [36].

The central role of the cGAS-STING pathway in pathogenic inflammation has invigorated extensive research into developing novel therapeutics modulating this pathway (recently reviewed in Ref. [37]). Despite the intense work, no STING inhibitor has yet advanced into the clinical stage, calling for additional discovery and development efforts for the unmet clinical need of targeting STING-dependent inflammation. Designing an inhibitor that binds to the ligand-binding domain of the dimeric STING is challenging due to the large volume of its binding pocket, requiring a bulky ligand with unfavorable drug molecular properties. It is also uncertain whether such a ligand would effectively inhibit STING variants with gain-of-function mutations. To circumvent it, we hypothesized that developing covalent modifiers that alkylate Cys88/91 to block STING palmitoylation would be an effective strategy against both wild-type and mutated STINGs, regardless of the conformation of the cyclic dinucleotide (CDN)-binding site [38]. Indeed, several Cys88/91 alkylating compounds have been reported in recent years. Using a library screen, the Ablasser group discovered nitrofuran analogs that covalently bind and inhibit STING [39]. Two chemical entities, C-176 and C-178, inhibit murine STING specifically, whereas modified compounds, C-170, C-171, and H-151, also inhibit human STING. These compounds inhibit STING signaling by covalently modifying Cys91 and preventing its palmitoylation [39]. At that time, we discovered that nitrated fatty acids, a class of endogenous lipid signaling species, inhibit STING signaling by preventing STING palmitoylation at Cys88 and Cys91 [40]. More recently, the Cravatt group identified that electrophilic acrylamide analogs BPK-21 and BPK-25 inhibit STING by targeting palmitoylation at Cys91 [41]. These recent discoveries highlight that inhibiting STING palmitoylation is a relevant pharmacological target to reduce STING-dependent inflammation.

The nitrated fatty acids are well-characterized bioactive lipids that exert a variety of anti-inflammatory and tissue-protective functions [42]. These electrophilic compounds react reversibly with cellular nucleophiles (e.g., reactive cysteine and histidine-containing proteins) of targeted proteins via Michael addition [43,44]. Nitroalkene-protein adducts will then transfer into glutathione (GSH) to be metabolized and excreted through the mercapturic acid pathway [45,46]. We discovered that the nitrated fatty acids could covalently modify STING by nitro-alkylating Cys88 and Cys91, thus preventing the essential palmitoylation required for STING activation and translocation [21], and inhibiting the downstream STING signaling and the subsequent release of type I IFNs. Furthermore, nitrated fatty acids are consistently generated endogenously in the gastrointestinal tract before systemic distribution [47–49]. They are also generated locally at inflammation sites, during ischemic events [50–52] and in response to viral infections [40]. This suggests that nitrated fatty acids constitute a naturally occurring feedback mechanism to restrain inflammation [53], and provide a scaffold to support the development of new-generation STING inhibitors.

Nitrooleic acid (NO_2-OA), a clinical candidate being evaluated in a Phase II clinical trial to treat obese asthmatics [54], became our prototypical nitrated fatty acids. Despite the high tolerance and promising efficacy, NO_2-OA showed a limited half-life and was rapidly deactivated through loss or migration of the double bond to form non-electrophilic 10-NO_2-stearic acid or 10-NO_2-octadec-8-enoic acid, respectively, limiting its half-life [54,55]. Additionally, nitrated fatty acids are absorbed and distributed in chylomicrons as triglyceride esters. This process results in low plasma concentrations (ng/mL) of the free and bioactive fatty acids [54,56]. We previously synthesized a small library of NO_2-OA-derived mimetics and evaluated their activity in the Nrf2 and NF-κB pathways, revealing that the chemical scaffold (e.g., spatial orientation and positions of the nitrovinyl group) plays a role in their biological activity, and metabolic inactivation [57].

Drawing from our prior experience and the hypothesis that chemical modifications of the nitrated fatty acid scaffold could enhance STING inhibition, we embarked on the design and synthesis of a novel series of chemical entities through iterative processes. These iterations involved constraining the degrees of freedom of the alkyl chain, adjusting the reactivity of the nitroalkene group, altering the hydrophobicity of the molecules, and tuning the steric hindrance of the ancillary moieties. The potential for inhibiting STING-dependent signaling was herein evaluated entirely in human cell models relevant to STING signaling. We tested if the lead nitroalkene compounds, CP-36 and CP-45, could modulate STING-dependent inflammation *in vivo*. The compounds showed a notable capacity to dampen both systemic and tissue-specific STING-dependent inflammation regardless of administration routes, with remarkable effects even after a single dose.

In summary, nitroalkenes target and strongly inhibit STING-dependent signaling. Thus, our study provides structural insight into STING inhibition by nitroalkenes. This knowledge can guide the development of drug candidates for more effective STING inhibition for treating autoimmune and autoinflammatory diseases where STING is a central driver of devastating inflammation.

2. Results

2.1. Comprehensive structure-activity relationship study of nitroalkene inhibition of STING

Nitrated oleic products, 9- and 10-nitrooleic acids, have been shown to inhibit STING [40]. To optimize the nitrated fatty acid chemical scaffold for STING inhibition, we first evaluated the impact on STING-dependent signaling using a small library of analogs in human cells. The *in-house* library is composed of nitroalkene acyl acids and fatty alcohols with varying chain lengths (14–24 carbons), and the nitrovinyl group is placed at distances ranging from as near as three carbons from the carboxyl group to the ω-end of the fatty acid chain (CP-1 to CP-16 and CP-18 to CP-21 in Supplementary Table 1) [57]. Nitroalkenes were first tested using NF-κB and IRF reporter assays in THP-1 dual cells featuring NF-κB-SEAP and IRF-Lucia luciferase. This allows simultaneous evaluation of the NF-κB and IRF-pathways by measuring SEAP and secreted luciferase, respectively. Several structure-activity relationship features were identified: a) the inhibition was abolished when nitroalkene fatty acids were shorter than 17 carbons (CP-1 to CP-3) or longer than 20 carbons (CP-13 to CP-16); b) the distance between the nitrovinyl group and the carboxyl group influences the activities with 7-NO_2 to 9-NO_2 alkenes providing the optimal spacing; and c) a

hydrophobic tail was essential for STING inhibition (Fig. 1A). We next tested the inhibition of CXCL-10, an interferon-induced cytokine, expression in THP-1 cells. Like the results obtained in the NF-κB and IRF reporter activity assay, CP-8 and CP-10 demonstrated a marked CXCL-10 reduction (Fig. 1B). As negative controls, oleic (OA) and linoleic acid (LA) did not suppress the response, showing that the activity was dependent on the presence of the nitroalkene group (Fig. 1A). As one of the most consistent STING inhibitors, we synthesized and evaluated individual isomers of CP-8 (7-NO_2-nonadec-7-enoic acid (CP-8a) and 8-NO_2-nonadec-7-enoic acid (CP-8b)). Both isomers demonstrated dose-dependent CXCL-10 inhibition, comparable to H-151 at a highest concentration tested (Fig. 1C). Nitrated fatty acids are largely metabolized to nitrodicarboxylates in humans, dogs, rats, and mice due to sequential ω-oxidation and various degrees of β-oxidation [46]. To evaluate whether dicarboxylate metabolites would retain the ability to inhibit STING, we synthesized a series of nitroalkene dicarboxylate esters (CP-23 to CP-30 in Supplementary Table 2), to promote cellular uptake as dicarboxylates are less cell-permeable. We found that the presence of an additional carboxyl group abolished the suppression of STING, suggesting that an aliphatic tail could be essential for STING nitroalkylation (Supplementary Fig. 1). To establish if other electrophilic compounds could inhibit STING, we tested the α,β-unsaturated keto electrophile, kynurenine-carboxyketoalkene (kyn-CKA, here just termed CKA). CKA, a non-nitroalkene endogenous electrophile, recently reported to exert anti-inflammatory activities [58], also failed to elicit STING inhibition (Fig. 1C). Next, we sought to establish that the anti-inflammatory effects were correlated to the suppression of the STING signaling pathway. The lead compounds, CP-6, CP-8a, CP-8b, and CP-10, efficiently suppressed phosphorylation of STING, TBK1, and IRF3, in a dose-dependent manner (Fig. 1D). On the contrary, the unrelated electrophilic species, CKA, and the nitroalkene diesters such as CP-25 did not retain this activity, suggesting the importance of the structural components of the compounds beyond their electrophilic warhead. Notably, no suppression on pSTING and pIRF3 was observed by H-151 either (Fig. 1D). As a result of IFN inhibition, NO_2OA and the CP-8s also impaired the induction of interferon-stimulated genes (ISGs), including IFIT1 and ISG15. In this case, the effect was mirrored by H-151 (Fig. 1E). Besides their ability to inhibit wild-type STING, we also evaluated the potential of the lead nitroalkene compounds for blocking the STING activity in SAVI patient-derived fibroblasts bearing the gain-of-function mutation N154S. By blocking the palmitoylation of STING, critical step of STING oligomerization and translocation, the selected nitroalkenes (i.e. CP-8s, CP-10 and CP-12) efficiently suppressed type I IFN release in a dose-dependent manner in SAVI fibroblast (Fig. 1F). This effect was again correlated with the suppression of pSTING, TBK1, and IRF3 in SAVI cells (Fig. 1G). Although H-151 also reduced IFN expression, the effect was not STING-dependent as pSTING, TBK1, or IRF3 were not altered in SAVI patient-derived fibroblasts. Collectively, several lead compounds in this generation (i.e., CP-6, CP-8, CP-10, CP-12) robustly reduced CXCL-10 and type I IFN levels prominently by inhibiting STING activity.

2.2. Conjugated nitroalkenes with favorable physicochemical properties amplify the STING inhibition

With the critical structural features learned from the initial screen, we engaged in compound optimization efforts, focusing on improving the nitroalkene electrophilicity and achieving greater specificity by reducing the degree of freedom in the molecules. Thus, a series of conjugated nitroalkenes (CP-33 to CP-58) were designed to achieve a more rigid molecular scaffold (Supplementary Table 3). Conjugated nitroalkenes, including aromatic rings, are reported to be strong electrophiles [59]. Additionally, the embedded aromatic ring was introduced to limit β-oxidation, a primary metabolic pathway. We also tested NO_2-eleostearic acid (NO_2-EA), a naturally occurring and endogenously formed compound recently found in human urine [60]. To assess the improved inhibition profiles and pharmacological characteristics of the second-generation nitroalkenes, we evaluated the *in vitro* therapeutic index based on the ability to suppress cGAMP-induced CXCL-10 release and cytotoxicity in THP-1s. Based on this assay, several conjugated nitroalkene compounds (i.e., CP-36, CP-45, CP-46, CP-50, CP-51, and NO_2-EA) strongly inhibited the cGAMP-induced CXCL-10 release while showing minimal cytotoxicity as assessed by MTT measurements (Fig. 2).

The STING inhibitory effects of these selected conjugated nitroalkene compounds were further evaluated in SAVI patient-derived fibroblasts bearing the gain-of-function mutation N154S. CP-36, CP-45, CP-46, and CP-50 reduced significantly and dose-dependently IFN expression while showing minimum cytotoxicity (Fig. 3A). The selected conjugated nitroalkenes (i.e., CP-36, CP-45, and CP-46) also efficiently suppressed the NF-κB and IRF reporter activity in THP-1 dual cells induced by cGAMP in a dose-dependent manner (Fig. 3B). Benchmarked against CP-8b, CP-36, and CP-50 also dose-dependently inhibited STING signaling, indicated by reduced STING, TBK1, and IRF3 phosphorylation in SAVI cells (Fig. 3C). To further characterize the electrophilic properties of the lead CP-36 and CP-45 compounds (nitroalkenes as in CP-8b have previously been characterized [44]), we evaluated their reactivity towards glutathione (GSH). The compounds have absorption peaks shifted to the right (323 nm and 333 nm for CP-36 and CP-45, respectively) compared to nitrooleic acid (268 nm) because of the increased conjugation conferred by the adjacent aromatic ring (Fig. 3D). Reaction with GSH, the most abundant intracellular thiol, resulted in a decrease in peak absorbance and a single isosbestic point formed at 275 nm for CP-36 and 279 nm for CP-45, suggesting that no intermediates accumulate and that the reaction proceeds in only one kinetically relevant step (Fig. 3D). To characterize the reaction, we performed a stopped-flow kinetic analysis of the reaction following the loss of absorbance at the compound's peak wavelength. The plots of the pseudo-first-order exponential constant (k_{obs}) against GSH concentration were linear, resulting in k_{on} second-order rate constants of 50.7 ± 0.6 $M^{-1}s^{-1}$ and 164 ± 1 $M^{-1}s^{-1}$ (25 °C, pH 7.4) for CP-36 and CP-45, respectively (Fig. 3E–F). A possible explanation for the lower rate constant of CP-36 is the presence of a negative charge at the reaction pH, which could slow the reaction with the also negatively charged GSH. In contrast, CP-45 is neutral. The y-intercepts of the linear regression of the k_{obs} versus GSH concentration plots were slightly below 0 for both compounds. While values below 0 are not expected from a kinetic perspective, the data likely indicate that the reaction of both compounds with GSH is irreversible or has a very small negligible k_{off} (Fig. 3F). This strongly contrasts with other prototypical nitroalkenes like nitrooleic acid and conjugated nitrolinoleic acid that display a reversible reaction with thiols. Nitrooleic acid has a lower k_{on} reaction constant (64 M^{-1} s^{-1}) than CP-45 and a higher k_{off} (0.006 s^{-1}) [44]. It could be speculated, that another distinctive characteristic of CP-36 and CP-45 is that they likely are not esterified to triglycerides and packed into chylomicrons for distribution, as reported for nitrated fatty acids [56]. The selected lead compounds in this generation were further evaluated in acute STING animal models.

2.3. Intraperitoneal administration of CP-36 dampens STING-dependent inflammation in vivo

To assess the STING inhibition of CP-36 *in vivo*, we injected a synthetic cGAMP analog, $cAIM(PS)_2$ Difluor (Rp/Sp), intraperitoneally into mice to induce STING-dependent systemic inflammation. Both CP-8b and CP-36 were initially selected for testing because of their ability to modulate STING activity and low toxicity in SAVI patient-derived fibroblasts (Supplementary Figs. 2A and 2B). Intraperitoneal administration of CP-8b was not well tolerated in mice. In contrast, CP-36 (both at low and high doses) was well tolerated and allowed for determining tissue-specific STING-dependent anti-inflammatory effects, as evaluated by *Ifnb1* gene expression and ISGs induction in various tissues. CP-36 administration improved protection against STING activation by

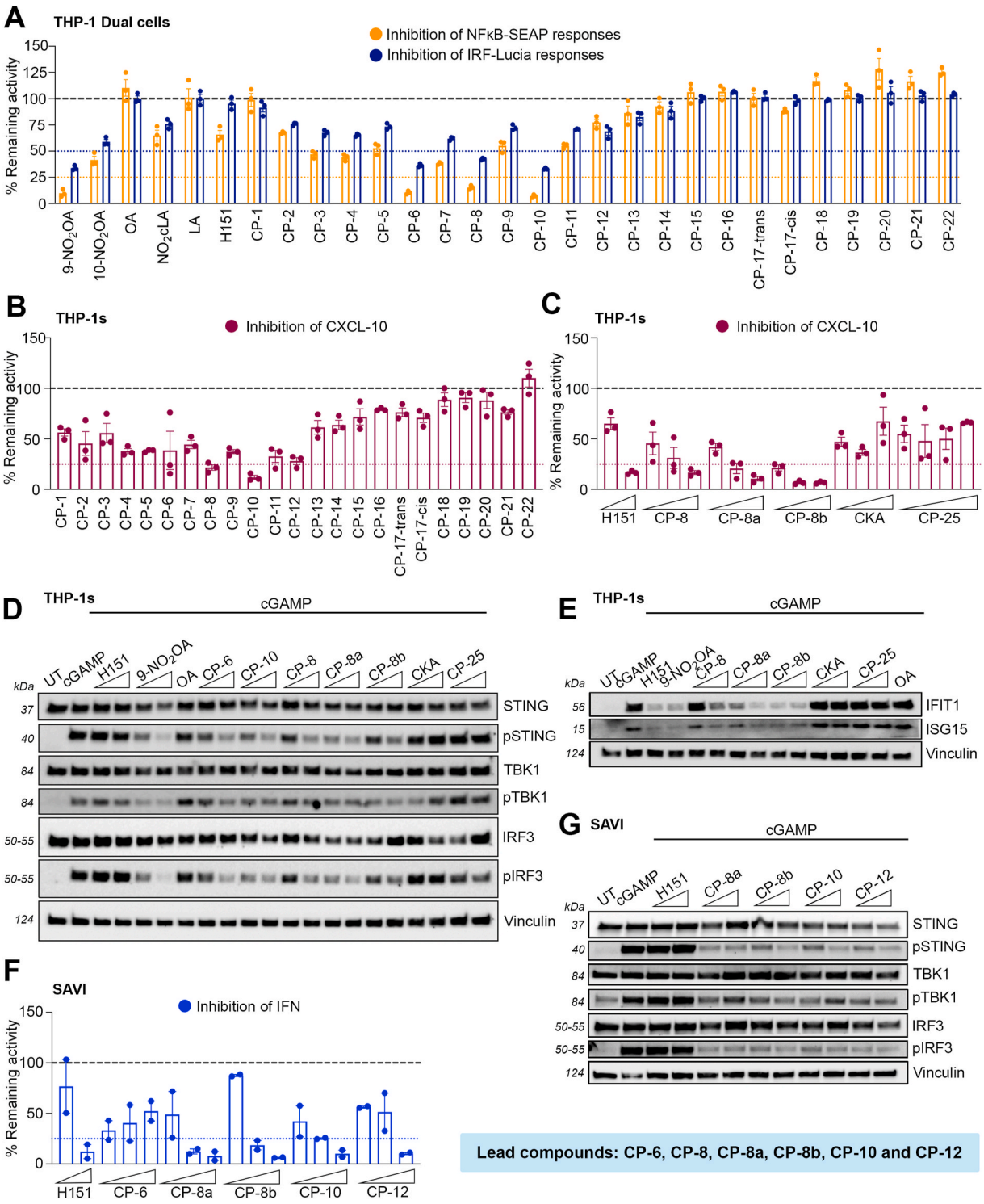

Fig. 1. Inhibition of STING by nitroalkene compounds depends on fatty acyl chain length and relative position of the nitroalkene group. The cells were pre-treated with specified concentrations of testing compounds for 2 h, followed by cGAMP stimulation (4 μg/mL) for 24 h (unless otherwise stated below) **(A)** Levels of NF-κB and IRF activation in THP-1-Dual cells treated with indicated nitroalkene compounds (10 μM) or H-151 (1 μM) and cGAMP stimulation. **(B)** CXCL-10 release in THP-1 wt cells treated with indicated nitroalkene compounds (10 μM). **(C)** CXCL-10 release in THP-1 wt cells treated with indicated nitroalkene compounds (2, 5 and 10 μM), CKA (15, 20 and 30 μM), and CP-25 (2, 5, 10 and 15 μM) or H-151 (0.5 and 1 μM). **(D)** Immunoblot analysis of whole-cell lysate of THP-1 wt cells to evaluate levels of STING, pSTING, TBK1, pTBK1, IRF3, and pIRF3 after treatment with indicated nitroalkene compounds (5 and 10 μM), OA (10 μM), CKA (20 and 30 μM), CP-25 (5 and 10 μM) or H-151 (0.5 and 1 μM), followed by 3 h cGAMP stimulation. **(E)** Immunoblot analysis of whole-cell lysate of THP-1 wt cells to evaluate levels of IFIT1 and ISG15 after treatment with indicated nitroalkene compounds (5 and 10 μM), 9-NO_2OA and OA (10 μM), CKA (20 and 30 μM), CP-25 (5 and 10 μM) or H-151 (1 μM). **(F)** Type I IFN release in SAVI fibroblasts treated with indicated nitroalkene compounds (1, 2 and 5 μM) or H-151 (2 and 5 μM). **(G)** Immunoblot analysis of whole-cell lysate of SAVI fibroblasts to evaluate levels of STING, pSTING, TBK1, pTBK1, IRF3 and pIRF3 after treatment with indicated nitroalkene compounds (5 and 10 μM) or H-151 (1 and 2 μM), followed by 3 h cGAMP stimulation. Bars indicate the mean ± SEM of two to three replicates and are normalized to the levels reached with cGAMP, expressed as a percentage. The dotted lines denote 75 % inhibition of NF-kB activation, CXCL-10 response, and type I IFN response, or 50 % inhibition of IRF activation of that induced by cGAMP.

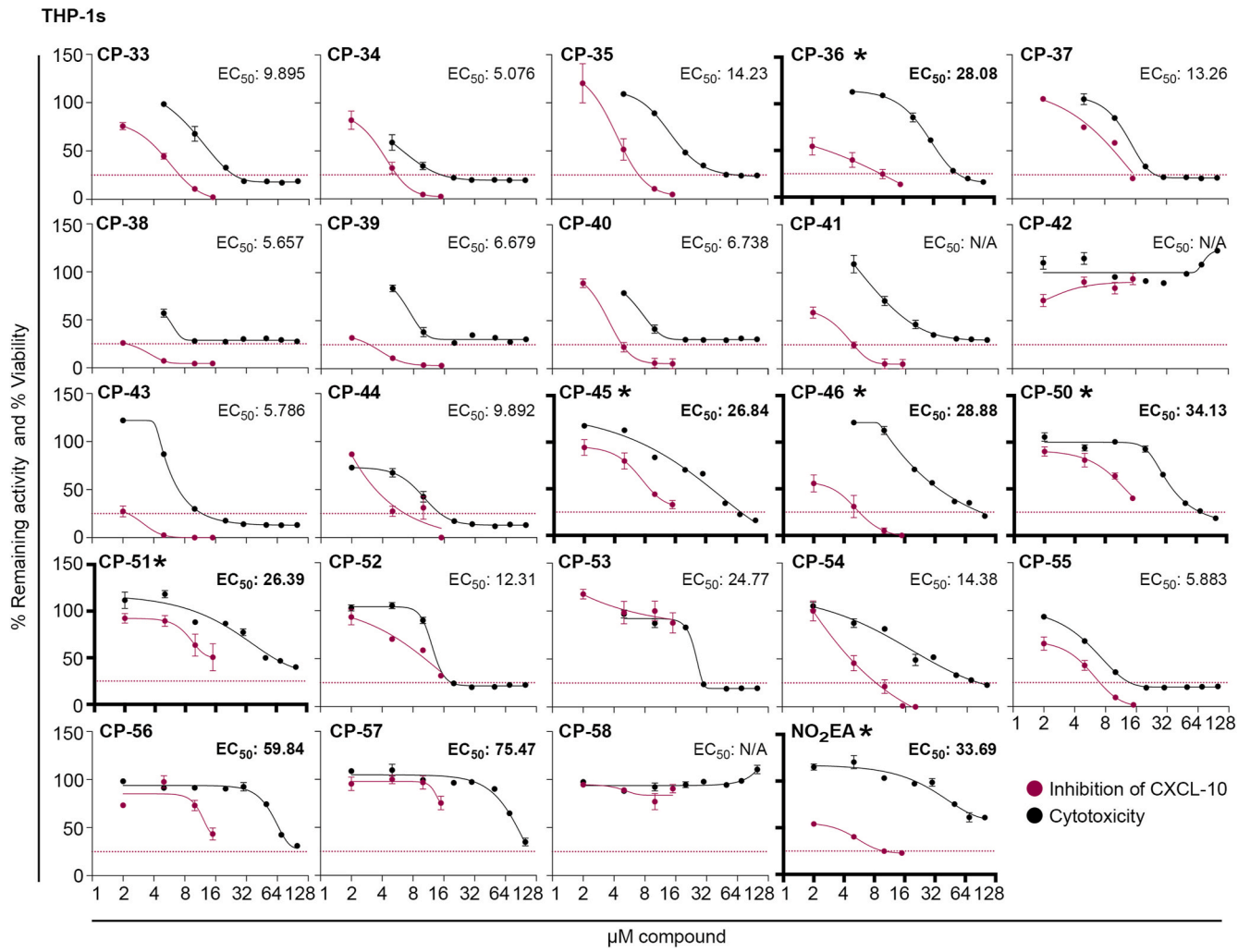

Fig. 2. Determining the *in vitro* therapeutic index of second-generation nitroalkene-based compounds. *In vitro* therapeutic index based on inhibition of CXCL-10 release plotted against level of cytotoxicity. For CXCL-10 release, THP-1 wt cells were pre-treated with indicated nitroalkene compounds in different concentrations (2, 5, 10 and 15 μM) for 2 h, followed by cGAMP stimulation (4 μg/mL) for 24 h. The cytotoxicity was measured by MTT assay, and THP-1 wt cells were treated with indicated nitroalkene compounds in different concentrations (2, 5, 10, 15, 20, 30, 50, 70 and 100 μM) for 24 h. Data of the therapeutic index represent the mean ± SEM of three replicates. The CXCL-10 release is normalized to the levels reached with cGAMP, expressed as a percentage. The dotted line denotes 75 % inhibition of the CXCL-10 response induced by cGAMP. The cytotoxicity is normalized to untreated cells, expressed as percentage viability. The EC_{50} value is determined by fitting the curve with nonlinear regression, and compounds with EC_{50} values above 25 are considered to have low cytotoxicity (bold numbers). The asterisk and bold axes indicate the lead compounds with a high *in vitro* therapeutical index, due to high potency to inhibit CXCL-10 production with minimal cytotoxicity.

dampening *Ifnb1* expression in several tissues, including the liver, lung, spleen, and heart (Supplementary Fig. 3B). While there appears to be a discernible trend in the protective effects, the large variability observed in the responses to the cGAMP analog undermined the ability to establish significant protection. A significantly larger *n* would be required to establish a statistical significance in *Ifnb1* expression. Nonetheless, CP-36 markedly decreased the expression of *Ifnb1* in the liver (Supplementary Fig. 3B). In addition, given the role of STING in lung inflammatory processes, we specifically evaluated the dampening of STING signaling pathways in the liver and lung. Here, we found statistically significant pTBK1, TBK1, and Viperin reductions in lung tissue (Fig. 4A&C) and STAT1 in liver tissue (Fig. 4B and C) with the 30 mg/kg CP-36 administration. As reported earlier, nitrated fatty acids rely on their electrophilicity to modulate STING activity, and nitroalkylating Cys88/91 blocks STING palmitoylation [40]. Therefore, we also synthesized a reduced CP-36 (R-CP-36) by saturating the nitroalkene into a nitroalkane as a negative control. The loss of electrophilicity in R-CP-36, implying loss of reactivity toward the Cys88/91, completely abolished the STING inhibition observed with CP-36 (Fig. 4D–F). CP-36 significantly decreased both *Ifnb1* and *Cxcl-10* expression in BDMDs, whereas R-CP-36 was completely ineffective (Fig. 4F). Additionally, only CP-36, rather than R-CP-36, exerts significant reductions of *Isg15* and *Ifit1* expression (Supplementary Fig. 4B). Moreover, the cGAMP induction of *Ifnb, Cxcl-10*, *Isg15,* and *Ifit1* expression is dependent on STING, while no response upon cGAMP stimulation was seen in bone marrow-derived macrophages (BMDMs) from STING knockout mice (Supplementary Figs. 4A and B). This indicates that the inhibition is specific to STING and requires the electrophilicity of the nitroalkene group.

Collectively, the conjugated nitroalkene, represented by CP-36, significantly mitigated the tissue-specific inflammation in STING-activated animals and relied on the electrophilic nitroalkene warhead to exert the STING inhibitory effects.

2.4. Oral administration of nitroalkene compounds CP-36 and CP-45 dampens STING-dependent inflammation in vivo

Oral bioavailability is a key characteristic in drug development as it

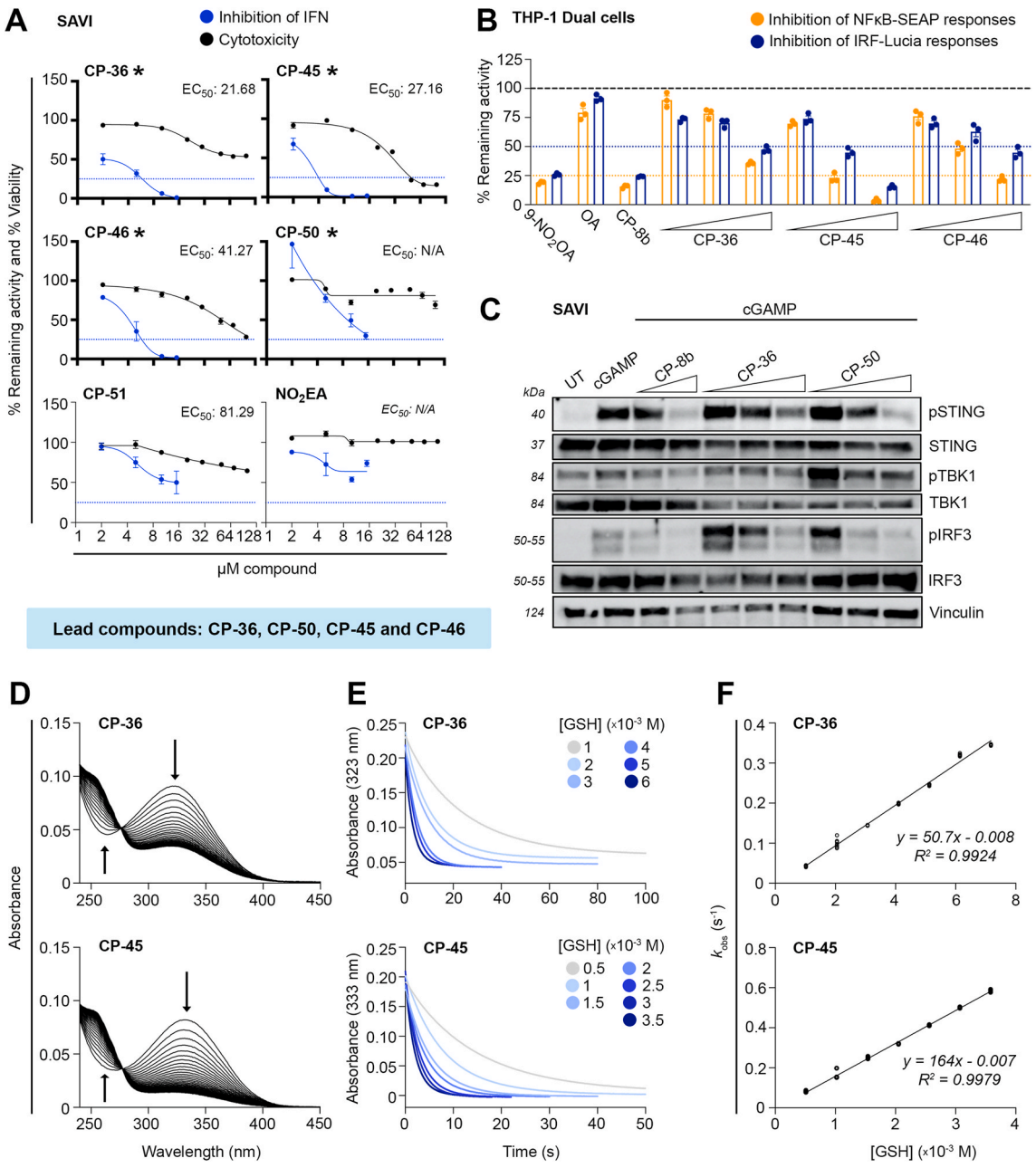

Fig. 3. Inhibition of STING by second-generation nitroalkene-based compounds and assessment of electrophilic characterization. (A) *In vitro* therapeutic index based on inhibition of type I IFN release plotted against level of cytotoxicity. For type I IFN release, SAVI fibroblasts were pre-treated with indicated nitroalkene compounds (2, 5, 10 and 15 μM) for 2 h, followed by cGAMP stimulation (4 μg/mL) for 24 h. The cytotoxicity was measured by MTT assay, SAVI fibroblasts were treated with indicated nitroalkene compounds in different concentrations (2, 5, 10, 15, 20, 30, 50, 70 and 100 μM) for 24 h. Data of the therapeutic index represent the mean ± SEM of two (IFN) and three (MTT) replicates. The type I IFN release is normalized to levels reached with cGAMP, expressed as percentage. The cytotoxicity is normalized to untreated cells, expressed as percentage viability. The dotted line denotes 75 % inhibition of the type I IFN response induced by cGAMP. The EC_{50} value is determined by fitting the curve with nonlinear regression. The asterisk and bold axes indicate the lead compounds with a high *in vitro* therapeutical index, due to high potency to inhibit type I IFN production with minimal cytotoxicity. **(B)** Level of NF-κB and IRF activation in THP-1-Dual cells after pre-treatment with indicated nitroalkene compounds (10, 20 and 30 μM) or 9-NO_2OA (10 μM), CP-8b (20 μM) and OA (30 μM) for 2 h, followed by cGAMP stimulation (4 μg/mL) for 24 h. Bars indicate the mean ± SEM of three replicates and are normalized to cGAMP levels, expressed as percentage. The dotted lines denote 50 % or 75 % inhibition of the IRF and NF-kB activation induced by cGAMP, respectively. **(C)** Immunoblot analysis of whole-cell lysate of SAVI fibroblasts to evaluate levels of pSTING, STING, pTBK1, TBK1, pIRF3 and IRF3 after treated with indicated nitroalkene compounds (2, 5 and 10 μM) or CP-8b (5 and 10 μM) for 2 h, followed by cGAMP stimulation (4 μg/mL) for 3 h. **(D–F)** Reaction kinetics of CP-36 (top panels) and CP-45 (bottom panels) with GSH. **(D)** Changes in UV–vis absorbance of CP-36 (10 μM) and CP-45 (10 μM) upon reaction with GSH (50 μM) in phosphate buffer (0.1 M, pH 7.4, 0.1 mM DTPA) at 25 °C. Spectra was recorded every 36 s for CP-36 and 12 s for CP-45, capturing approximately 10 half-lives of the reaction between GSH and the nitroalkene. The downward arrows at 323 and 333 nm indicate consumption of CP-36 and CP-45, respectively. The upward arrows at 265/270 nm indicate the formation of a single adduct with GSH **(E)** Stopped flow kinetic traces of the reaction of CP-36 (20 μM) and CP-45 (μM) with increasing concentrations of GSH, followed at 323 and 333 nm, respectively. **(F)** Exponential pseudo-first order rate constants as a function of GSH concentration. K_{obs} values were determined from the best fit of the kinetics traces shown in **(E)** to a single-phase exponential with slope function and plotted against GSH concentration.

significantly increases the reach of the therapeutic approach. To compensate for any loss in drug absorption and bioavailability compared to intraperitoneal (i.p.), we elevated the oral dosage of the administered nitroalkene compounds to 40 mg/kg and 60 mg/kg. Given that CP-8b i.p. administration was not well tolerated, we incorporated CP-45 alongside CP-36 in subsequent *in vivo* experiments using oral delivery. CP-45 demonstrated a favorable therapeutic index in earlier patient-derived SAVI cell evaluations, and it is structurally distinctive from CP-36, with the carboxyl group positioned on the same side as the nitroalkene (Supplementary Figs. 2A and 2B). Furthermore, as a methyl ester, CP-45 is expected to exhibit improved passive intestinal absorption compared to its carboxylic parent compound.

First, we assessed if CP-36 and CP-45 were absorbed and systemically distributed. For CP-45, only the de-methylated metabolite was assessed, as the determination of the methyl ester by HPLC-MS/MS and GC-MS/MS posed challenges, including very low sensitivity due to the lack of ionizable groups (LC) and enhanced degradation during work-up and heating (GC). Consequently, the CP-45 levels were significantly lower than CP-36, likely indicating limited hydrolysis of the ester. Similar to nitrated fatty acids, both CP-36 and CP-45 were found to be deactivated by a reductase *in vivo*, potentially prostaglandin reductase 1 (a phase II metabolic enzyme) [55], to give rise to their reduced forms (dihydro-CP-36, R-CP-36 and dihydro-CP-45, R-CP-45) (Supplementary Figs. 5A and B).

Next, we examined the capability of CP-36 and CP-45 to inhibit tissue-specific STING-dependent inflammation by assessing both the STING signaling pathway and the induction of interferon-stimulated genes (ISGs). Our findings revealed a strong and statistically significant reduction in STAT1 levels in lung tissue (Fig. 5A and B, Supplementary Fig. 6A). We also observed a significant effect on STING and phosphorylated STING upon administration of CP-45, whereas Viperin was mostly reduced by 40 mg/kg CP-36. Notably, no variance in ISG15 levels was detected (Fig. 5A and B, Supplementary Figs. 6A and B). Moreover, we observed a comparable trend of inhibition of the STING-dependent inflammation in the liver tissue (Supplementary Figs. 7A and B). Then, we wanted to evaluate if CP-36 and CP-45 could systemically inhibit STING-dependent inflammation. We observed an overall reduction of relevant inflammatory cytokines and chemokines (e.g., for IFN-α, IFN-β, MCP-1, and MIP-1β) upon administration of 60 mg/kg CP-36 and CP-45, though a high animal variability in the responses to the activator (Fig. 5C). We also observed an overall suppression of TNF-α and CXCL-10 upon administering 40 mg/kg CP-36. Lastly, a statistically significant reduction was seen in MCP-1 levels with 40 mg/kg CP-36 and in TNF-α levels with 60 mg/kg CP-45 (Fig. 5C). Collectively, single doses of CP-36 and CP-45 dampened STING-dependent inflammatory cytokines and chemokines systemically and demonstrated substantial protection against cGAMP-induced STING-dependent inflammation.

3. Discussion

Aberrant activation of STING signaling is associated with a range of autoimmune and autoinflammatory conditions such as STING-associated vasculopathy with onset in infancy (SAVI) [35]. SAVI patients present with severe symptoms, including early-onset systemic inflammation, severe skin vasculopathy and interstitial lung disease, ultimately causing pulmonary fibrosis and respiratory failure [35]. Currently, there are no clinically available therapeutics directly targeting the STING signaling, let alone treatment options for SAVI patients or those experiencing other inflammatory conditions resulting from gain-of-function STING mutations [36]. Many STING inhibitors have been developed to target the cyclic dinucleotide (CDN)-binding domain to prevent cGAMP binding, thereby reducing the downstream signaling of the cGAS-STING pathway [37]. However, the V155M and N154S mutations of SAVI patients are assumed to cause STING to adopt a more closed conformation and become constitutively active, regardless of CDN binding [35,61]. Therefore, those inhibitors may not be effective for STING with gain-of-function mutations. Thus, inhibiting palmitoylation of Cys88/91, which facilitates STING translocation and oligomerization, could represent a more robust strategy to suppress STING signaling in both normal and SAVI conditions. In recent years, several compounds targeting the essential STING palmitoylation event at Cys88/91 [38] have been identified, such as inhibitors containing reactive electrophilic nitroalkene [40], nitrofuran, indole urea [39], and acrylamide groups [41]. These compounds have been tested in diverse *in vivo* [39,62–64] and *ex vivo* [65] models to evaluate their pre-clinical treatment potential in inhibiting inflammation such as STING-dependent inflammatory processes. Recent discoveries of additional compounds, such as BB-Cl-amidine targeting STING oligomerization through Cys148 modification [66], underscore the growing interest in inhibiting STING and the potential and effectiveness of covalent modulators.

Here, we screened nitroalkene compounds for their potential to inhibit STING-dependent signaling and inflammation. The *in vitro* therapeutical potential of the nitroalkene compounds was determined by measuring their ability to suppress type I IFN and CXCL-10 release, NFκB/IRF activation, and STING signaling, in addition to assessing levels of cytotoxicity. This process enabled us to identify several lead nitroalkene compounds capable of inhibiting STING signaling, with conjugated nitroalkenes emerging as potent inhibitors while displaying minimal cytotoxicity. The structure-activity findings allowed us to identify optimal inhibitors for blocking STING activation. Furthermore, we tested the ability of lead nitroalkene compounds, CP-36 and CP-45, to modulate STING-dependent inflammation *in vivo*. First, CP-36, when administered intraperitoneally, effectively mitigated tissue-specific STING-dependent inflammation through its electrophilic properties, as no effect was observed with the deactivated analog R-CP-36. Subsequently, both lead nitroalkene compounds, CP-36 and CP-45, significantly dampened tissue-specific and systemic STING-dependent inflammation *in vivo* when administrated orally. Notably, the inhibitory effect was observed after a single dose and was independent of the administration route. The acute inflammation model employed in our study served as a proof-of-concept experiment designed to demonstrate target engagement and the initial efficacy of CP-36 and CP-45 in inhibiting STING activation. Further studies to validate the therapeutic potential of these inhibitors would involve models of chronic over-activation of the cGAS-STING pathway. Using the Trex1-deficient mouse models of Aicardi-Goutières syndrome (AGS) [67,68] or the hSTING-N154S mouse model of SAVI [69] would more accurately assess the compounds' ability to alleviate the persistent inflammatory state observed in human autoinflammatory diseases. To demonstrate the broader therapeutic impact and translational potential of STING inhibition, disease-specific models for Systemic Lupus Erythematosus (SLE) [70], cardiovascular diseases [71] and age-related neurogenerative disorders [72] will provide critical insights into the efficacy of STING inhibitors across a spectrum of chronic conditions where the cGAS-STING pathway plays a pathogenic role.

Overall, we observed a dose-dependent damping effect upon intraperitoneal and oral administration. One of the pharmacological characteristics of electrophilic modifiers is that they exhibit a bell-shaped dose-response curve, losing efficacy at high doses. This phenomenon has been widely described and has also been observed in preclinical models using nitro fatty acids [73]. Adequate dosing of electrophiles such as nitroalkene compounds is a critical component for successful *in vivo* studies and should be considered in future evaluation of the lead compounds identified in this study.

In a recent study, a very limited therapeutical effect of H-151 was observed. The authors of that study speculate that an extremely low oral bioavailability (F = 0.6 %) and a very short half-life of H-151 could be the reason [74]. Our findings revealed that the H-151 could strongly reduce the expression of CXCL-10, type I IFN, and ISGs *in vitro*. However, its impact on STING signaling components such as pSTING, pTBK1, and pIRF3 seemed minimal in THP-1s and SAVI fibroblasts. This disparity

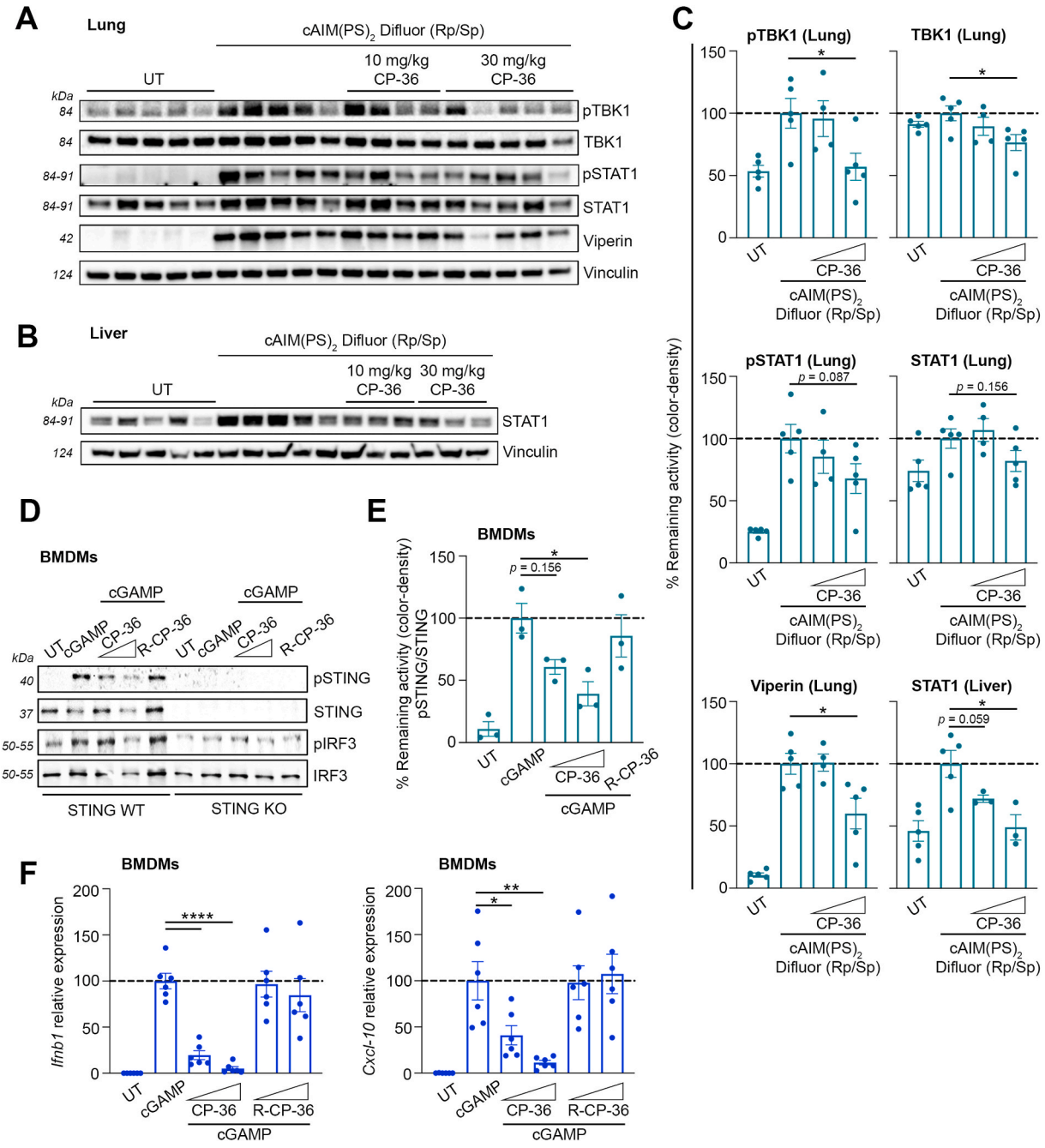

Fig. 4. Intraperitoneal administration of nitroalkene compound CP-36 dampens STING-dependent inflammation *in vivo*. **(A–C)** Mice were administrated with CP-36 i.p. (10 or 30 mg/kg) 2 h before activating STING with i.p. injection of cAIM(PS)$_2$ Difluor (Rp/Sp) (0.2 mg/kg) for 4 h. Immunoblot analysis of homogenized and lysed **(A)** lung and **(B)** liver tissue to evaluate the levels of pTBK1, TBK1, pSTAT1, STAT1 and Viperin with **(C)** densitometry quantification of protein levels. The plots include data from individual mice represented in immunoblots. Bars indicate mean ± SEM and are normalized to the cAIM(PS)$_2$ Difluor (Rp/Sp) group, expressed as a percentage. **(D–F)** WT or STING-KO BMDMs were pre-treated with CP-36 (5 and 10 μM) or reduced CP-36 (R-CP-36, 5 and 10 μM) for 2 h, followed by cGAMP stimulation (4 μg/mL) for either 3 h or 6 h. **(D)** Immunoblot analysis of whole-cell lysate (representative blot) to evaluate levels of pSTING, STING, pIRF3 and IRF3 and **(E)** densitometry quantification of pSTING/STING protein levels after 3 h cGAMP stimulation. Three independent experiments are plotted. **(F)** qPCR analysis of *Ifnb1* and *Cxcl-10* expression was quantified relative to *18S* mRNA levels after 6 h of cGAMP stimulation. BMDM cultures obtained from 6 individual mice (3 male and 3 female mice) are plotted. Bars indicate mean ± SEM and are normalized to cGAMP levels, expressed as a percentage. Statistical analyses were performed using Welch's *t*-test, yielding the following *p* values: For tissues: pTBK1: $p = 0.0293$, TBK1: $p = 0.0283$, Viperin: $p = 0.0311$, STAT1: $p = 0.0159$. For BMDMs: pSTING/STING: $p = 0.0184$, *Ifnb1*: $p < 0.0001$, *Cxcl-10*: *, $p = 0.0367$ and **, $p = 0.0076$. * Indicates $p < 0.05$, ** indicates $p < 0.01$, and **** indicates $p < 0.0001$.

might stem from H-151's potential inability to achieve or sustain adequate concentrations in the cytoplasm for effective inhibition of STING activation and downstream signaling. Another plausible explanation is that H-151 may exhibit varying affinities or specificities for different STING variants or mutants, resulting in diverse responses to the inhibitor. Moreover, both CP-36 and CP-45 reacted with GSH with a high degree of irreversibility in comparison to nitrated fatty acids [44]. However, our study clearly demonstrates that these compounds inhibit STING activity, suggesting a higher reaction rate constants with STING cysteines and/or preferential binding of the nitroalkene compounds to

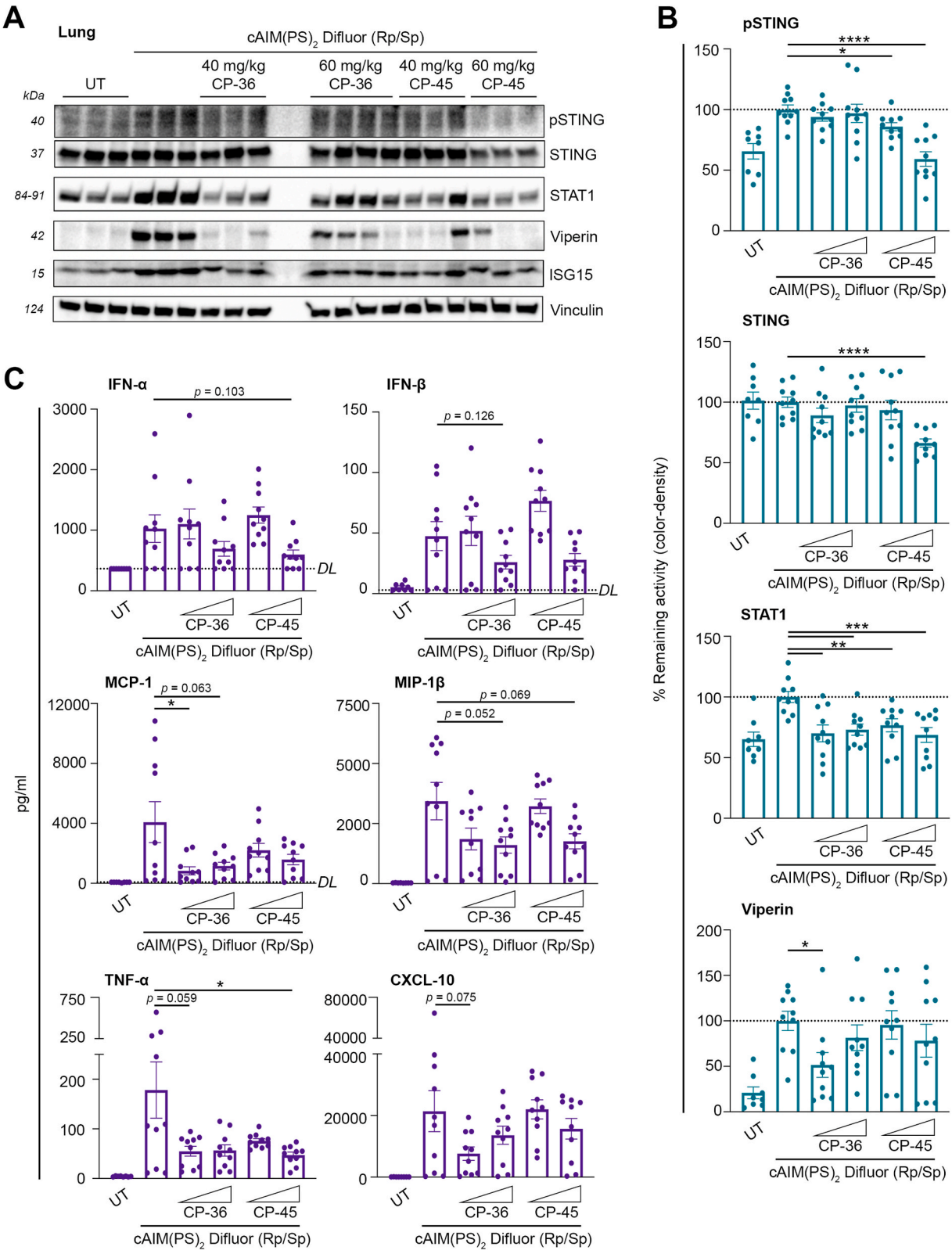

Fig. 5. Oral administration of nitroalkene compounds CP-36 and CP-45 dampens STING-dependent inflammation *in vivo*. Mice were administrated with CP-36 and CP-45 orally (40 or 60 mg/kg) for 2 h before activating STING with i.p. injection of cAIM(PS)$_2$ Difluor (Rp/Sp) (0.2 mg/kg) for 4 h. **(A)** Immunoblot analysis of homogenized and lyzed lung tissue to evaluate the levels of pSTING, STING, STAT1, Viperin and ISG15 tissue (representative blot) with **(B)** densitometry quantification of protein levels. **(C)** Cryo-preserved plasma was analyzed for levels of IFNα, IFNβ, MCP-1, MIP-1β, TNFα, and CXCL-10 using Meso Scale Discovery. DL signifies the Detection Limit for individual assays. Individual mice are plotted. Bars indicate mean ± SEM and are normalized to the cAIM(PS)$_2$ Difluor (Rp/Sp) group, expressed as a percentage. Statistical analyses by Welch's *t*-test. *P* values: MCP-1: $p = 0.0429$, TNF-α: $p = 0.0464$, pSTING: *, $p = 0.0126$ and ****, $p < 0.0001$, STING: $p < 0.0001$, STAT1: **, $p = 0.0024$ (CP-36, 40 mg/kg) and $p = 0.0042$ (CP-45, 40 mg/kg) and ***, $p = 0.0006$ (CP-36, 60 mg/kg) and $p = 0.0008$ (CP-45, 60 mg/kg), and Viperin: $p = 0.0122$. * Indicates $p < 0.05$, ** indicates $p < 0.01$, *** indicates $p < 0.001$, and **** indicates $p < 0.0001$.

STING. Thus, our study underscores the substantial therapeutic potential of the nitroalkene compounds CP-36 and CP-45 as potent STING inhibitors with improved pharmacokinetic properties compared to H-151.

The safety and proven anti-inflammatory properties of nitroalkenes, as supported by the concluded (NCT03422510, NCT04053543, and NCT03449524) and ongoing (NCT03762395) Phase II clinical trials underscore their potential as therapeutic compounds. These clinical studies predominantly focused on the anti-inflammatory actions of nitrated fatty acids, particularly their roles in NFκB inhibition and Nrf2 activation. The positive safety and tolerability outcomes of nitrated fatty acids in clinical testing further highlight the therapeutic promise of nitroalkene compounds, providing a strong foundation for the preclinical development of the conjugated nitroalkenes identified as lead compounds in this study. Nonetheless, long-term administration of STING inhibitors needs to be evaluated during the preclinical and clinical development phase. As STING has important functions in the host defense against pathogens, the long-term use of STING inhibitors for treating autoinflammatory conditions may raise concerns due to the heightened risk of infectious complications. Exemplified by anifrolumab (Saphnelo™), an IFN receptor antibody used for SLE treatment, common side effects include upper respiratory tract infections and bronchitis in addition to viral re-activation (EMA, European Medicines Agency). Thus, it will be crucial to maintain vigilant monitoring for adverse effects, especially in immune-compromised patients, to maintain a favorable risk-benefit balance. As STING also plays an important role in maintaining gut homeostasis [75], long-term inhibition of STING might affect its function in the homeostatic response to commensal microbiome. Thus, exploring targeted delivery systems for STING inhibitors holds promise for minimizing systemic exposure, thereby improving treatment precision and safety. Lastly, comprehensive pharmacokinetic and pharmacodynamic profiling will play a vital role in establishing optimal dosing strategies for sustained therapy, ensuring both efficacy and safety over the long-term administration of STING inhibitors.

In summary, our study concludes that conjugated nitroalkene compounds, distinguished by their electrophilicity and pharmacokinetics, robustly target and inhibit STING-dependent signaling. Through this research, we have advanced our understanding of the optimal structure-activity relationship for designing covalent modifiers that block STING activity. These findings serve as a foundation for the research and development of clinical STING inhibitors, offering potential treatments for several autoimmune and autoinflammatory diseases where STING plays a pivotal role.

4. Methods

Cells and culture conditions. Human acute monocytic leukemia cell line, THP-1s wt cells (ATCC, RRID:CVCL_0006) and NF-κB-SEAP and IRF-Lucia luciferase Reporter Monocytes, THP-1-Dual cells (InvivoGen, RRID: CVCL_X599) were cultured in RPMI 1640 (Sigma-Aldrich) supplemented 10 % heat inactivated Fetal Bovine Serum (FBS, Sigma-Aldrich), 100 Units/mL penicillin, 100 μg/mL streptomycin, and 292 μg/mL glutamine (P–S-G, Gibco) (hereafter termed complete RPMI). The THP-1-Dual cells were further supplemented with 100 μg/mL Normocin in addition to 10 μg/mL Blasticidin, and 100 μg/ml Zeocin at every second passage (InvivoGen). To differentiate THP-1s wt into adherent macrophages, cells were stimulated with 100 nM phorbol 12-myristate 13-acetate (PMA, Sigma-Aldrich) for 24 h in complete RPMI before the medium was replaced with complete RPMI without PMA and cells were allowed to further differentiate for one additional day before experiments. HEK-Blue IFN-α/β cells (InvivoGen, RRID:CVCL_KT26) were cultured in DMEM supplemented with 10 % heat-inactivated FBS (Sigma-Aldrich) and P–S-G (Gibco) (hereafter termed complete DMEM) further supplemented with 30 μg/mL Blasticidin, 100 μg/mL Normocin and 100 μg/mL Zeocin (InvivoGen). Fibroblasts isolated from a patient suffering from STING-associated vasculopathy with onset in infancy (SAVI) bearing the mutation in the coding region, c.461A > G, of STING (TMEM173) leading to an Asn to Ser substitution in protein, p.N154S were kindly provided by Raphaela Goldbach-Mansky (RGM, NIH, Bethesda, USA) and cultured in complete DMEM using a 50 % media change at passing and seeded 48 h prior to experiments. Passing of HEK-Blue IFN-α/β cells and SAVI fibroblasts was done using 0.25 % Trypsin (Gibco) supplemented with 0.3 mM EDTA (Invitrogen). All cell cultures were kept at 37 °C, 5 % CO_2, and cell lines were regularly tested for mycoplasma contamination by sequencing from GATC Biotech (Germany).

SAVI Fibroblasts. Primary fibroblasts from the SAVI patient were obtained from superficial skin biopsies [35]. The patient with genetically confirmed SAVI was enrolled into the protocol (clinicaltrials.gov: NCT02974595) at the NIH between 2008 and 2015. The protocol was approved by the National Institute of Allergy and Infectious Diseases IRB at the NIH. Written informed consent was obtained from the patient or their legal guardians (RGM).

Animals. For *in vivo* experiments with intraperitoneally (i.p.) administration, nine weeks old pathogen-free C57BL/6JRj (WT) male mice were bred at the animal vendor Janvier Labs (France). Experiments were carried out at Aarhus University. Prior to experiments, mice were allowed to acclimatize, and animals received proper care in agreement with animal protocols approved by Animal Welfare Bodies at Health, Aarhus University and conducted with ethical permission from the Animal Experiments Inspectorate, Danish Veterinary and Food Administration (permission#: 2016-15-0201-01072) to perform i.p. injections. The study was carried out in strict accordance with the recommendations in the Guide for the Care and Use of Laboratory Animals, EEC Council Directive 2010/63/EU. For *in vivo* experiments with oral gavage administration, 12 weeks old pathogen-free C57BL/6J male mice (RRID: IMSR_JAX:000664) were maintained in a temperature- and light-controlled environment (12-h light/dark cycle) at Morehouse School of Medicine Center for Laboratory Animal Resources (CLAR) and were fed standard diet (PicoLab rodent diet 5LOD; LabDiet) and water ad libitum. Animal experiments were approved by the Institutional Animal Care and Use Committee of Morehouse School of Medicine (21-06) and performed in accordance with institutional guidelines. For the BMDM experiments, male and female C57BL/6J (RRID: IMSR_JAX:000664) and STING knockout mice (RRID:IMSR_JAX:025805) (12 weeks old) were maintained at Morehouse School of Medicine CLAR under above-described conditions and regulations.

BMDMs. For the bone marrow-derived macrophages (BMDMs), the mouse L-929 (RRID:CVCL_0462) conditioned medium was used as a source of colony-stimulating factor activity. The L-929 cells were grown in RPMI supplemented with 10 % FBS with fresh medium added every 3 days (20 % v/v). After 10 days, the culture medium was removed, filtered (0.22 p.m. filter), and used for BMDM cultures. The BMDMs were obtained from bone marrow cells from C57BL/6J and STING knockout mice by flushing the marrow from femurs with RPMI containing 10 % FBS. The marrow plugs were disrupted into a single cell suspension, cultured in RPMI containing 10 % FBS supplemented with 15 % L-929 cell-conditioned medium at a density of 1×10^6 cells. After 7 days, adherent BMDM cells were washed with PBS and medium replaced with RPMI, 1 % FBS, 15 % L-929 cell-conditioned medium overnight.

Screening compounds. The cellular screening used both commercially available compounds and *in-house* synthesized novel nitroalkene. The commercially available compounds included STING inhibitor H-151 (InvivoGen), nitrated oleic acids 9-NO_2OA and 10-NO_2OA, along with non-nitrated control lipids oleic acid (OA) and linoleic acid (LA) (Cayman Chemicals). Whereas the *in-house* synthesized novel nitroalkenes, listed in Supplementary table 1, 2 and 3, in addition to reduced nitroalkene as negative controls. All compounds were dissolved in DMSO (CKA in MetOH). Cells were pre-treated with the testing compounds for 2 h before stimulation. Appropriate control vehicles consisting of EtOH, DMSO or MetOH were used.

Synthesis of nitroalkene compounds. See *Supplementary information*.

cGAMP stimulation. The STING agonist, 2′3′-cGAMP (InvivoGen) was used for intracellular stimulation using Lipofectamine2000 (Lipo, Invitrogen). cGAMP and Lipo were diluted in serum-free medium with a ratio of Lipo/cGAMP of 1:1 and the final concentration of cGAMP was 4 μg/mL and lipo alone was used as mock treatment. For BMDM experiments, the STING activation was done using 2′3′-cGAMP sodium salt (Tocris) and Lipoefectamine2000 (ThermoFischer Scientific).

***In vivo* administration of compounds and cGAMP.** For *in vivo* administration of compounds, the synthesized nitroalkenes were gently warmed to obtain an oily form, weighed out, and further mixed with Polyethylene glycol (PEG400, Sigma-Aldrich) (2/3 of final volume) and next 1/3 volume of saline was added before being administrated. For intraperitoneally (i.p.) injections, the compounds (10 or 30 mg/kg) were formulated in the above described PEG400/saline mixture. The same formulation of testing compounds (40 or 60 mg/kg) was applied for oral administration. The PEG400/saline mixture was also used for mock treatment in both the i.p. and oral administration. For *in vivo* activation of STING, the Rp/Sp-isomers of the bisphosphorothioate derivative of cAIMP, an analog of the bacterial cyclic dinucleotide 3′3′-cGAMP (cAIM $(PS)_2$ Difluor (Rp/Sp), CL656, InvivoGen) [76] were diluted in saline (InvivoGen) and administrated by i.p. injections at 0.2 mg/kg and mock treatment was performed with saline. One mouse in the 10 mg/kg CP-36 group was excluded from all downstream analyses due to inappropriate STING activation based on Viperin protein levels in the lung (Supplementary Fig. 3A).

Sample collection and preparation. After sacrifice, whole blood was harvested to Microvette 500, EDTA K3 tubes (Sarstedt) and stored at room temperature (RT) until processing. Plasma was harvested after 1500×*g* centrifugation for 15 min and cryopreserved at −80 °C until analysis. Next, the heart was perfused with saline to rinse the heart and lungs before tissue harvest. Both whole organs or smaller organ pieces were snap-frozen using dry ice and stored at −80 °C until further processing.

MTT assay. To evaluate cytotoxicity, the colorimetric Cell Proliferation Kit I (MTT-based) (Roche) was used according to the manufacturer's recommendations. The absorbance of the formazan product was measured at 550 nm on Synergy HTX multimode reader (BioTEK).

Cytokine and Type I IFN measurements. Human CXCL-10 was quantified by DuoSet ELISA Development System (R&D Systems) according to the manufacturer's recommendations and absorbance was read at 450 nm on Synergy HTX multimode reader (BioTEK). Human type I IFN was quantified using the reporter cell line HEK-Blue™ IFN-α/β reporter cells by the manufacturer's instructions (InvivoGen, RRID: CVCL_KT26). Using QUANTI-Blue the SEAP levels were determined by reading the OD at 630 nm on Synergy HTX multimode reader (BioTEK).

Multiplex cytokine analysis by Meso Scale Discovery. Two customized, high-sensitive 3- and 4-cytokine U-plex panels (Meso Scale Discover (MSD) were used to analyze plasma levels of IFNα, IFNβ, MIP-1β and TNFα (4-plex) and CXCL-10, MCP-1, and IL-6 (3-plex) in the cryopreserved plasma according to the manufacturer's protocol. Data were acquired using a QuickPlex SQ 120 instrument (MSD, Rockville, MD, USA). The lower limit of quantification of individual assays was as follows IFN-α: 490.19 pg/ml; IFN-β: 2.898 pg/ml, MIP-1β: 19.81 pg/ml, TNF-α: 0.1234 pg/ml; CXCL-10: 0.643 pg/ml; MCP-1: 1.973 pg/ml, and IL-6: 2.18 pg/ml.

NF-κB/IRF reporter assay. The NF-κB-SEAP (secreated embryonic alkaline phosphatase) and IRF-Lucia luciferase Reporter Monocytes, THP-1-Dual cells (InvivoGen, RRID:CVCL_X599) were used according to the manufacturer's recommendation. NF-κB and IRF activation were assessed by measuring the levels of SEAP and Lucia luciferase using QUANTI-Blue and QUANTI-Luc, respectively. Levels of SEAP were determined by reading the OD at 630 nm, and those of Lucia luciferase were determined by measuring the relative light units (RLUs) in a luminometer. Both readings were conducted on the Synergy HTX multimode reader (BioTEK).

Stopped flow kinetic studies. Kinetics studies were performed using an Applied Photophysics SX20 stopped-flow approaches. CP-36 or CP-45 were individually mixed with increasing concentrations of GSH (0.001–0.0035 M) in phosphate buffer (0.1 M, pH 7.4, DTPA 0.1 mM) at 25 °C. Absorbance was recorded over time at 323 and 333 nm for CP-36 and CP-45, respectively, as these are the maximal absorbances in phosphate buffer for each compound. As a control, no changes in absorbance were observed in the absence of GSH, except for slight photobleaching. Single exponential plus linear functions were fit to the reaction time courses. The exponential pseudo-first order rate constants k_{obs} were plotted against GSH concentration and the second-order rate constants were determined from the slopes. GSH concentration was verified by titration with 5,5′-dithiobis(2-nitrobenzoate) using an absorption coefficient at 412 nm of 14,150 M^{-1} cm^{-1} for the product [77]. GSH stocks were prepared in phosphate buffer (0.1 M, pH 7.4, DTPA 0.1 mM) and the pH was adjusted with KOH to the same pH of the buffer.

Western Blot. *In vitro* preparation of samples was as follows, 400,000 THP-1s wt cells or 100,000 SAVI fibroblasts were lysed in 100 or 50 μl, respectively, ice-cold Pierce RIPA lysis buffer (Thermo Fischer Scientific) supplemented with 10 mM NaFlouride, 1X cOmplete EDTA-free Protease Inhibitor Cocktail (Roche) and 50 units/mL Benzonase (Sigma-Aldrich) (hereafter termed complete lysis buffer). Similarly, a small piece of tissue was first homogenized in complete lysis buffer using steel beads and the TissueLyser II (Qiagen). Lysates were pelleted and the supernatants were sonicated using the Bioruptor (Diagenode). The protein concentration was determined using Pierce BCA protein assay kit (Thermo Fischer Scientific). Whole-cell or tissue lysates were denatured for 3 min at 95 °C in the presence of XT Sample Buffer and XT reducing agent (BioRad). A total of 10 μg of reduced samples was separated by SDS-PAGE on 4–20 % Criterion TGX precast gradient gels (BioRad). Each gel was run initially for 15 min at 70 V, followed by 45 min at 110 V. Transfer onto midi 0.2 μM PVDF membranes (BioRad) was done using a Trans-Blot Turbo Transfer system (BioRad) for 7 min. Membranes were blocked for 1 h with 5 % skim milk (Merck Millipore) at RT in PBS supplemented with 0.05 % Tween-20 (PBS-T). Membranes were fractionated in smaller pieces and probed overnight at 4 °C with any of the following specific primary antibodies were used 1:1000 in PBS-T with 0.05 % NaAzide for the *in vitro* samples: anti-STING (Cell Signaling Technology (CST) Cat# 13647, RRID:AB_2732796), anti-phospho-STING (CST Cat# 19781, RRID:AB_2737062), anti-TBK1/NAK (CST Cat# 3013, RRID:AB_2199749), anti-phospho-TBK1/NAK (CST Cat# 5483, RRID:AB_10693472), anti-IRF3 (CST Cat# 11904, RRID:AB_2722521), anti-phospho-IRF3 (Ab76493, Abcam, RRID: AB_1523836), anti-IFIT1(CST Cat# 14769, RRID:AB_2783869), anti-ISG15 (CST Cat# 2758, RRID:AB_2126200) and anti-Vinculin CST Cat# 18799, CST, RRID:AB_2714181) as loading control. In addition to the above listed, the following specific primary antibodies were used 1:1000 in PBS-T with 0.05 % NaAzid for the *in vivo* samples: anti-Viperin (Millipore Cat# MABF106, RRID:AB_11203644), anti-STAT1 (CST cat# 14994, RRID:AB_2737027), anti-phopho-STAT1 (CST Cat# 14994, RRID:AB_2737027). After three washes in PBS-T, secondary antibodies, Peroxidase AffiniPure F(ab')2 Donkey anti-mouse IgG (H + L) or peroxidase AffiniPur F(ab')2 Donkey anti-rabbit IgG (H + L) (Jackson ImmunoResearch) were added used 1:10,000 in PBS-T 1 % milk for 1 h at room temperature. All membranes were washed three times in PBS-T and exposed using either the SuperSignal West Pico PLUS Chemiluminescent Substrate or the SuperSignal West Femto Maximum Sensitivity Substrate (Thermo Fischer Scientific) and Image Quant LAS4000 mini-imager (GE Healthcare) or Azure 300 imager (Azure Biosystems). For the BMDM experiments, cells were lysed in Tissue Protein Extraction Reagent (T-PER, Thermo Scientific) supplemented with a protease inhibitor cocktail (Roche Applied Science). Protein extracts were resolved in 10 % SDS–PAGE gels and transferred to nitrocellulose membranes (Bio-Rad). After blocking in TBST containing 5 % non-fat dry milk at room temperature for 1 h, membranes were immunoblotted with primary antibodies at 4 °C overnight. The following antibodies were used: Phospho-STING (D8F4W) (CST Cat# 72971, RRID:AB_2799831; 1:500);

Phospho-IRF-3 (4D4G) (CST Cat# 4947, RRID:AB_823547; 1:500), STING (D2P2F) (CST Cat# 13647, RRID:AB_2732796, 1:1000); IRF3 (D83B9) (CST Cat# 4302, RRID: AB_1904036, 1:1000); GAPDH (14C10) (CST Cat# 2118, RRID: AB_561053, 1:1000). The membranes were washed by TBST before incubated with Goat Anti-Rabbit IgG (H L)-HRP Conjugate secondary antibody (RRID: AB_11125142, 1:5000) at room temperature for 1h followed by signal detection using Clarity Western ECL Substrate (Bio-Rad). Western blots were scanned and quantified using an iBright FL1500 Imager (ThermoFisher Scientific). Nitrocellulose membranes were stripped from primary and secondary antibodies using Restore™ Western Blot Stripping Buffer (ThermoFisher Scientific) for 15 min and re-probed following the above antibody order. The levels of proteins were quantified by densitometry using the AzureSpot Pro software (Azure Biosystems) or NIH Image J.

qPCR analysis. For *in vivo* experiments, smaller pieces of tissues (approx. 25 mg) were homogenized in Buffer RLT Plus (Qiagen) using steel beads and TissueLyser II (Qiagen). Lysates were pelleted and RNA isolated from supernatants using qPCR RNeasy Mini kit with either on-column DNase digestion or gRNA eliminator spin columns (Qiagen) following manufacturer's protocol. RNA quality was assessed by NanoDrop spectrometry (Thermo Fischer Scientific). Gene expression was determined by real-time quantitative PCR (qPCR) using and TaqMan detection systems (Applied Biosystems). RNA levels for murine *Ifnb1* (Mm00439552_s1) and *Actb* (Mm02619580_g1) were analyzed using premade TaqMan assays and the RNA-to-Ct-1-Step kit according to manufacturer's recommendations. Samples were analyzed in technical duplicates and appropriate controls were included. Expression levels were quantified relative to beta-actin expression, using the $2_t^{-\Delta\Delta C}$ method [78] and normalized to the cGAMP group as a fold change. For BMDM experiments, total RNA was extracted using Aurum Total RNA Mini Kit (Bio-Rad). RNA quantity was determined using NanoDrop spectrometry (ThermoFisher Scientific). RNA was reverse transcribed into cDNA using random primers with GoScript Reverse Transcriptase System (Promega). Specific transcript levels for murine *Ifnb1* (forward primer: 5′ CAG CTC CAA GAA AGG ACG AAC 3′, reverse primer: 5′ GGC AGT GTA ACT CTT CTG CAT 3′), *Cxcl-10* (forward primer: 5′ CCA AGT GCT GCC GTC ATT TTC 3′, reverse primer: 5′ TCC CTA TGG CCC TCA TTC TCA 3′), *Ifit1* (forward primer: 5′ CTG AGA TGT CAC TTC ACA TGG AA 3′, reverse primer: 5′ GTG CAT CCC CAA TGG GTT CT 3′), *Isg15* (forward primer: 5′ GGT GTC CGT GAC TAA CTC CAT 3′, reverse primer: 5′ TGG AAA GGG TAA GAC CGT CCT 3′) and *18S* (forward primer: 5′ GGA AGG GCA CCA CCA GGA GT 3′, reverse primer: 5′ TGC AGC CCC GGA CAT CTA G 3′) were assessed by a CFX Connect Real-Time PCR Detection System (Bio-Rad) using iQ SYBR Green Supermix (Bio-Rad) and the ΔΔCt threshold cycle method of normalization. Gene expression levels were quantified relative to the expression of 18S and normalized to the cGAMP group as a fold change.

Statistics. Figures and statistical analyses were performed using GraphPad Prism version 10.1.1. The Welch's *t*-test was used to determine statistical significance.

CRediT authorship contribution statement

Fei Chang: Writing – review & editing, Writing – original draft, Methodology, Investigation, Data curation, Conceptualization. **Camilla Gunderstofte:** Investigation, Formal analysis, Data curation. **Nicole Colussi:** Writing – review & editing, Methodology, Investigation, Formal analysis. **Mareena Pitts:** Investigation. **Sonia R. Salvatore:** Investigation. **Anne L. Thielke:** Investigation. **Lucia Turell:** Writing – review & editing, Methodology, Investigation, Formal analysis. **Beatriz Alvarez:** Writing – review & editing, Methodology, Investigation, Formal analysis. **Raphaela Goldbach-Mansky:** Resources, Methodology. **Luis Villacorta:** Writing – review & editing, Writing – original draft, Investigation, Funding acquisition, Formal analysis, Conceptualization. **Christian K. Holm:** Writing – review & editing, Writing – original draft, Supervision, Funding acquisition, Data curation, Conceptualization. **Francisco J. Schopfer:** Writing – review & editing, Writing – original draft, Methodology, Funding acquisition, Data curation, Conceptualization. **Anne Louise Hansen:** Writing – review & editing, Writing – original draft, Visualization, Supervision, Project administration, Methodology, Investigation, Funding acquisition, Formal analysis, Data curation, Conceptualization.

Declaration of competing interest

The authors declare the following financial interests/personal relationships which may be considered as potential competing interests:

Francisco J Schopfer reports a relationship with Creegh Pharmaceuticals Inc that includes: board membership and equity or stocks. Francisco J Schopfer & Fei Chang reports a relationship with Furanica Inc that includes: board membership and equity or stocks. Christian K Holm reports a relationship with UV Medico that includes: consulting or advisory and employment. Francisco J Schopfer, Fei Chang, Christian K Holm, Anne Louise Hansen, Sonia R Salvatore, Luis Villacorta are the inventors of a patent application related to the subject matter of this manuscript. The University of Pittsburgh is the lead institution for this patent application, with joint ownership also held by Aarhus University and Morehouse School of Medicine. Other authors declare that they have no known competing financial interests or personal relationships that could have appeared to influence the work reported in this paper.

Data availability

Data will be made available on request.

Acknowledgements

This work was supported by a PreSeed programme grant from Bio-Innovation Institute; a non-profit foundation supported by the Novo Nordisk Foundation. FJS was supported by NIH R01 GM125944. CKH was supported by Hørslev-Fonden. LV was supported by NIH grant R01-HL123333 and the National Center for Advancing Translational Sciences from NIH UL1TR002378. ALH was supported by a Lundbeck Foundation PostDoc Fellowship and Beckett-Fonden. MP was supported by the William Porter Physiology fellowship from the American Physiological Society. We thank Pascal Rowart, formerly at the University of Pittsburgh and Martin Kristian Thomsen, Aarhus University, for advising on *in vivo* experiments.

Appendix A. Supplementary data

Supplementary data to this article can be found online at https://doi.org/10.1016/j.redox.2024.103202.

References

[1] X. Zhang, H. Shi, J. Wu, X. Zhang, L. Sun, C. Chen, et al., Cyclic GMP-AMP containing mixed phosphodiester linkages is an endogenous high-affinity ligand for STING, Mol Cell 51 (2) (2013) 226–235.
[2] E.J. Diner, D.L. Burdette, S.C. Wilson, K.M. Monroe, C.A. Kellenberger, M. Hyodo, et al., The innate immune DNA sensor cGAS produces a noncanonical cyclic dinucleotide that activates human STING, Cell Rep. 3 (5) (2013) 1355–1361.
[3] A. Ablasser, M. Goldeck, T. Cavlar, T. Deimling, G. Witte, I. Rohl, et al., cGAS produces a 2'-5'-linked cyclic dinucleotide second messenger that activates STING, Nature 498 (7454) (2013) 380–384.
[4] P. Gao, M. Ascano, Y. Wu, W. Barchet, B.L. Gaffney, T. Zillinger, et al., Cyclic [G(2',5')pA(3',5')p] is the metazoan second messenger produced by DNA-activated cyclic GMP-AMP synthase, Cell 153 (5) (2013) 1094–1107.
[5] L. Sun, J. Wu, F. Du, X. Chen, Z.J. Chen, Cyclic GMP-AMP synthase is a cytosolic DNA sensor that activates the type I interferon pathway, Science 339 (2013) 786–791.
[6] J. Wu, L. Sun, X. Chen, F. Du, H. Shi, C. Chen, et al., Cyclic GMP-AMP is an endogenous second messenger in innate immune signaling by cytosolic DNA, Science 339 (6121) (2013) 826–830.
[7] H. Ishikawa, G.N. Barber, STING is an endoplasmic reticulum adaptor that facilitates innate immune signalling, Nature 455 (7213) (2008) 674–678.

[8] H. Ishikawa, Z. Ma, G.N. Barber, STING regulates intracellular DNA-mediated, type I interferon-dependent innate immunity, Nature 461 (7265) (2009) 788–792.
[9] W. Sun, Y. Li, L. Chen, H. Chen, F. You, X. Zhou, et al., ERIS, an endoplasmic reticulum IFN stimulator, activates innate immune signaling through dimerization, Proc Natl Acad Sci U S A. 106 (21) (2009) 8653–8658.
[10] L. Jin, P.M. Waterman, K.R. Jonscher, C.M. Short, N.A. Reisdorph, Cambier JC. Mpys, A novel membrane tetraspanner, is associated with major histocompatibility complex class II and mediates transduction of apoptotic signals, Mol. Cell Biol. 28 (16) (2008) 5014–5026.
[11] B. Zhong, Y. Yang, S. Li, Y.Y. Wang, Y. Li, F. Diao, et al., The adaptor protein MITA links virus-sensing receptors to IRF3 transcription factor activation, Immunity 29 (4) (2008) 538–550.
[12] N. Dobbs, N. Burnaevskiy, D. Chen, V.K. Gonugunta, N.M. Alto, N. Yan, STING activation by translocation from the ER is associated with infection and autoinflammatory disease, Cell Host Microbe 18 (2) (2015) 157–168.
[13] S. Srikanth, J.S. Woo, B. Wu, Y.M. El-Sherbiny, J. Leung, K. Chupradit, et al., The Ca(2+) sensor STIM1 regulates the type I interferon response by retaining the signaling adaptor STING at the endoplasmic reticulum, Nat. Immunol. 20 (2) (2019) 152–162.
[14] B.C. Zhang, R. Nandakumar, L.S. Reinert, J. Huang, A. Laustsen, Z.L. Gao, et al., STEEP mediates STING ER exit and activation of signaling, Nat. Immunol. 21 (8) (2020) 868–879.
[15] G. Shang, D. Zhu, N. Li, J. Zhang, C. Zhu, D. Lu, et al., Crystal structures of STING protein reveal basis for recognition of cyclic di-GMP, Nat. Struct. Mol. Biol. 19 (7) (2012) 725–727.
[16] Y.H. Huang, X.Y. Liu, X.X. Du, Z.F. Jiang, X.D. Su, The structural basis for the sensing and binding of cyclic di-GMP by STING, Nat. Struct. Mol. Biol. 19 (7) (2012) 728–730.
[17] S. Ouyang, X. Song, Y. Wang, H. Ru, N. Shaw, Y. Jiang, et al., Structural analysis of the STING adaptor protein reveals a hydrophobic dimer interface and mode of cyclic di-GMP binding, Immunity 36 (6) (2012) 1073–1086.
[18] C. Shu, G. Yi, T. Watts, C.C. Kao, P. Li, Structure of STING bound to cyclic di-GMP reveals the mechanism of cyclic dinucleotide recognition by the immune system, Nat. Struct. Mol. Biol. 19 (7) (2012) 722–724.
[19] P. Gao, M. Ascano, T. Zillinger, W. Wang, P. Dai, A.A. Serganov, et al., Structure-function analysis of STING activation by c[G(2',5')pA(3',5')p] and targeting by antiviral DMXAA, Cell 154 (4) (2013) 748–762.
[20] S.L. Ergun, D. Fernandez, T.M. Weiss, L. Li, STING Polymer structure reveals mechanisms for activation, Hyperactivation, and inhibition, Cell 178 (2) (2019) 290–301 e10.
[21] K. Mukai, H. Konno, T. Akiba, T. Uemura, S. Waguri, T. Kobayashi, et al., Activation of STING requires palmitoylation at the Golgi, Nat. Commun. 7 (2016) 11932.
[22] C. Zhang, G. Shang, X. Gui, X. Zhang, X.C. Bai, Z.J. Chen, Structural basis of STING binding with and phosphorylation by TBK1, Nature 567 (7748) (2019) 394–398.
[23] B. Zhao, F. Du, P. Xu, C. Shu, B. Sankaran, S.L. Bell, et al., A conserved PLPLRT/SD motif of STING mediates the recruitment and activation of TBK1, Nature 569 (7758) (2019) 718–722.
[24] S. Liu, X. Cai, J. Wu, Q. Cong, X. Chen, T. Li, et al., Phosphorylation of innate immune adaptor proteins MAVS, STING, and TRIF induces IRF3 activation, Science 347 (6227) (2015) aaa2630.
[25] B. Zhao, C. Shu, X. Gao, B. Sankaran, F. Du, C.L. Shelton, et al., Structural basis for concerted recruitment and activation of IRF-3 by innate immune adaptor proteins, Proc Natl Acad Sci U S A. 113 (24) (2016) E3403–E3412.
[26] Y. Tanaka, Z.J. Chen, STING Specifies IRF3 phosphorylation by TBK1 in the cytosolic DNA signaling pathway, Sci. Signal. 5 (214 ra20) (2012) 1–11.
[27] D.B. Stetson, R. Medzhitov, Recognition of cytosolic DNA activates an IRF3-dependent innate immune response, Immunity 24 (1) (2006) 93–103.
[28] C.C. de Oliveira Mann, M.H. Orzalli, D.S. King, J.C. Kagan, A.S.Y. Lee, P. J. Kranzusch, Modular Architecture of the STING C-terminal tail allows interferon and NF-kappaB signaling Adaptation, Cell Rep. 27 (4) (2019) 1165–11675 e5.
[29] T. Abe, G.N. Barber, Cytosolic-DNA-mediated, STING-dependent proinflammatory gene induction necessitates canonical NF-kappaB activation through TBK1, J. Virol. 88 (10) (2014) 5328–5341.
[30] X. Gui, H. Yang, T. Li, X. Tan, P. Shi, M. Li, et al., Autophagy induction via STING trafficking is a primordial function of the cGAS pathway, Nature 567 (7747) (2019) 262–266.
[31] D.B. Stetson, J.S. Ko, T. Heidmann, R. Medzhitov, Trex1 prevents cell-intrinsic initiation of autoimmunity, Cell 134 (4) (2008) 587–598.
[32] N. Jeremiah, B. Neven, M. Gentili, I. Callebaut, S. Maschalidi, M.C. Stolzenberg, et al., Inherited STING-activating mutation underlies a familial inflammatory syndrome with lupus-like manifestations, J. Clin. Invest. 124 (12) (2014) 5516–5520.
[33] Z. Deng, Z. Chong, C.S. Law, K. Mukai, F.O. Ho, T. Martinu, et al., A defect in COPI-mediated transport of STING causes immune dysregulation in COPA syndrome, J. Exp. Med. 217 (11) (2020).
[34] I. Melki, Y. Rose, C. Uggenti, L. Van Eyck, M.L. Fremond, N. Kitabayashi, et al., Disease-associated mutations identify a novel region in human STING necessary for the control of type I interferon signaling, J. Allergy Clin. Immunol. 140 (2) (2017) 543–552 e5.
[35] Y. Liu, A.A. Jesus, B. Marrero, D. Yang, S.E. Ramsey, G.A.M. Sanchez, et al., Activated STING in a vascular and pulmonary syndrome, N. Engl. J. Med. 371 (6) (2014) 507–518.
[36] Y. Dai, X. Liu, Z. Zhao, J. He, Q. Yin, Stimulator of interferon genes-associated vasculopathy with onset in infancy: a systematic review of case reports, Front Pediatr 8 (2020) 577918.
[37] A. Decout, J.D. Katz, S. Venkatraman, A. Ablasser, The cGAS-STING pathway as a therapeutic target in inflammatory diseases, Nat. Rev. Immunol. 21 (9) (2021) 548–569.
[38] A.L. Hansen, K. Mukai, F.J. Schopfer, T. Taguchi, C.K. Holm, STING palmitoylation as a therapeutic target, Cell. Mol. Immunol. 16 (3) (2019) 236–241.
[39] S.M. Haag, M.F. Gulen, L. Reymond, A. Gibelin, L. Abrami, A. Decout, et al., Targeting STING with covalent small-molecule inhibitors, Nature 559 (7713) (2018) 269–273.
[40] A.L. Hansen, G.J. Buchan, M. Ruhl, K. Mukai, S.R. Salvatore, E. Ogawa, et al., Nitro-fatty acids are formed in response to virus infection and are potent inhibitors of STING palmitoylation and signaling, Proc Natl Acad Sci U S A. 115 (33) (2018) E7768–E7775.
[41] E.V. Vinogradova, X. Zhang, D. Remillard, D.C. Lazar, R.M. Suciu, Y. Wang, et al., An activity-Guided Map of electrophile-cysteine interactions in primary human T cells, Cell 182 (4) (2020) 1009–1026 e29.
[42] T. Cui, F.J. Schopfer, J. Zhang, K. Chen, T. Ichikawa, P.R. Baker, et al., Nitrated fatty acids: endogenous anti-inflammatory signaling mediators, J. Biol. Chem. 281 (47) (2006) 35686–35698.
[43] L.M. Baker, P.R. Baker, F. Golin-Bisello, F.J. Schopfer, M. Fink, S.R. Woodcock, et al., Nitro-fatty acid reaction with glutathione and cysteine. Kinetic analysis of thiol alkylation by a Michael addition reaction, J. Biol. Chem. 282 (42) (2007) 31085–31093.
[44] L. Turell, D.A. Vitturi, E.L. Coitino, L. Lebrato, M.N. Moller, C. Sagasti, et al., The chemical basis of thiol addition to nitro-conjugated linoleic acid, a protective cell-signaling lipid, J. Biol. Chem. 292 (4) (2017) 1145–1159.
[45] S.R. Salvatore, D.A. Vitturi, P.R. Baker, G. Bonacci, J.R. Koenitzer, S.R. Woodcock, et al., Characterization and quantification of endogenous fatty acid nitroalkene metabolites in human urine, J. Lipid Res. 54 (7) (2013) 1998–2009.
[46] S.R. Salvatore, D.A. Vitturi, M. Fazzari, D.K. Jorkasky, F.J. Schopfer, Evaluation of 10-nitro oleic acid bio-elimination in rats and humans, Sci. Rep. 7 (2017) 39900.
[47] S.R. Salvatore, P. Gomez-Cortes, P. Rowart, S.R. Woodcock, M. Angel de la Fuente, F. Chang, et al., Digestive interaction between dietary nitrite and dairy products generates novel nitrated linolenic acid products, Food Chem. 437 (Pt 1) (2024) 137767.
[48] G. Bonacci, P.R. Baker, S.R. Salvatore, D. Shores, N.K. Khoo, J.R. Koenitzer, et al., Conjugated linoleic acid is a preferential substrate for fatty acid nitration, J. Biol. Chem. 287 (53) (2012) 44071–44082.
[49] M. Delmastro-Greenwood, K.S. Hughan, D.A. Vitturi, S.R. Salvatore, G. Grimes, G. Potti, et al., Nitrite and nitrate-dependent generation of anti-inflammatory fatty acid nitroalkenes, Free Radic. Biol. Med. 89 (2015) 333–341.
[50] L. Villacorta, L. Minarrieta, S.R. Salvatore, N.K. Khoo, O. Rom, Z. Gao, et al., In situ generation, metabolism and immunomodulatory signaling actions of nitro-conjugated linoleic acid in a murine model of inflammation, Redox Biol. 15 (2018) 522–531.
[51] V. Rudolph, T.K. Rudolph, F.J. Schopfer, G. Bonacci, S.R. Woodcock, M.P. Cole, et al., Endogenous generation and protective effects of nitro-fatty acids in a murine model of focal cardiac ischaemia and reperfusion, Cardiovasc. Res. 85 (1) (2010) 155–166.
[52] A.R. Mathers, C.D. Carey, M.E. Killeen, S.R. Salvatore, L.K. Ferris, B.A. Freeman, et al., Topical electrophilic nitro-fatty acids potentiate cutaneous inflammation, Free Radic. Biol. Med. 115 (2018) 31–42.
[53] F.J. Schopfer, N.K.H. Khoo, Nitro-fatty acid logistics: formation, biodistribution, signaling, and pharmacology, Trends Endocrinol Metab 30 (8) (2019) 505–519.
[54] R.M. Garner, D.R. Mould, C. Chieffo, D.K. Jorkasky, Pharmacokinetic and pharmacodynamic effects of oral CXA-10, a nitro fatty acid, after single and multiple ascending doses in healthy and obese subjects, Clin Transl Sci 12 (6) (2019) 667–676.
[55] D.A. Vitturi, C.S. Chen, S.R. Woodcock, S.R. Salvatore, G. Bonacci, J.R. Koenitzer, et al., Modulation of nitro-fatty acid signaling: prostaglandin reductase-1 is a nitroalkene reductase, J. Biol. Chem. 288 (35) (2013) 25626–25637.
[56] M. Fazzari, D.A. Vitturi, S.R. Woodcock, S.R. Salvatore, B.A. Freeman, F. J. Schopfer, Electrophilic fatty acid nitroalkenes are systemically transported and distributed upon esterification to complex lipids, J. Lipid Res. 60 (2) (2019) 388–399.
[57] N.K.H. Khoo, L. Li, S.R. Salvatore, F.J. Schopfer, B.A. Freeman, Electrophilic fatty acid nitroalkenes regulate Nrf2 and NF-kappaB signaling:A medicinal chemistry investigation of structure-function relationships, Sci. Rep. 8 (1) (2018) 2295.
[58] M.P.M. Carreño, S.R. Woodcock, T. Brzoska, S. Ghosh, S.R. Salvatore, F. Chang, N. K.H. Khoo, M. Dunn, N. Connors, S. Yuan, A.C. Straub, S.G. Wendell, G.J. Kato, B. A. Freeman, S.F. Ofori-Acquah, P. Sundd, F.J. Schopfer, D.A. Vitturi, Immunomodulatory Actions of a Kynurenine-Derived Endogenous Electrophile, 2022.
[59] J. Rodriguez-Duarte, R. Dapueto, G. Galliussi, L. Turell, A. Kamaid, N.K.H. Khoo, et al., Electrophilic nitroalkene-tocopherol derivatives: synthesis, physicochemical characterization and evaluation of anti-inflammatory signaling responses, Sci. Rep. 8 (1) (2018) 12784.
[60] S.R. Salvatore, P. Rowart, F.J. Schopfer, Mass spectrometry-based study defines the human urine nitrolipidome, Free Radic. Biol. Med. 162 (2021) 327–337.
[61] M.L. Fremond, Y.J. Crow, STING-mediated lung inflammation and beyond, J. Clin. Immunol. 41 (3) (2021) 501–514.
[62] F.J. Schopfer, M.P. Cole, A.L. Groeger, C.S. Chen, N.K. Khoo, S.R. Woodcock, et al., Covalent peroxisome proliferator-activated receptor gamma adduction by nitro-fatty acids: selective ligand activity and anti-diabetic signaling actions, J. Biol. Chem. 285 (16) (2010) 12321–12333.

[63] S. Borniquel, E.A. Jansson, M.P. Cole, B.A. Freeman, J.O. Lundberg, Nitrated oleic acid up-regulates PPARgamma and attenuates experimental inflammatory bowel disease, Free Radic. Biol. Med. 48 (4) (2010) 499–505.
[64] L. Villacorta, L. Chang, S.R. Salvatore, T. Ichikawa, J. Zhang, D. Petrovic-Djergovic, et al., Electrophilic nitro-fatty acids inhibit vascular inflammation by disrupting LPS-dependent TLR4 signalling in lipid rafts, Cardiovasc. Res. 98 (1) (2013) 116–124.
[65] A.L. Hansen, L.S.J. Rahbek, A.S. Sorensen, M.P. Hundahl, S. Lomholt, C.K. Holm, et al., Nitro-fatty acids decrease type I interferons and monocyte chemoattractant protein 1 in ex vivo models of inflammatory arthritis, BMC Immunol. 22 (1) (2021) 77.
[66] F. Humphries, L. Shmuel-Galia, Z. Jiang, J.Y. Zhou, L. Barasa, S. Mondal, et al., Targeting STING oligomerization with small-molecule inhibitors, Proc Natl Acad Sci U S A. 120 (33) (2023) e2305420120.
[67] J.L. Grieves, J.M. Fye, S. Harvey, J.M. Grayson, T. Hollis, F.W. Perrino, Exonuclease TREX1 degrades double-stranded DNA to prevent spontaneous lupus-like inflammatory disease, Proc Natl Acad Sci U S A. 112 (16) (2015) 5117–5122.
[68] M. Morita, G. Stamp, P. Robins, A. Dulic, I. Rosewell, G. Hrivnak, G. Daly, D. E. Barnes, Gene-targeted mice lacking the Trex1 (DNase III) 3′→5′ DNA exonuclease develop inflammatory myocarditis, Mol. Cell Biol. 24 (15) (2004) 6719–6727.
[69] G.R. Martin, K. Henare, C. Salazar, T. Scheidl-Yee, L.J. Eggen, P.P. Tailor, et al., Expression of a constitutively active human STING mutant in hematopoietic cells produces an Ifnar1-dependent vasculopathy in mice, Life Sci. Alliance 2 (3) (2019).
[70] A.M. Hagiwara, R.E. Moore, D.J. Wallace, M. Ishimori, C.A. Jefferies, Regulation of cGAS-STING pathway - implications for systemic lupus erythematosus, Rheumatol Immunol Res 2 (3) (2021) 173–184.
[71] B.P. Daniels, S.B. Kofman, J.R. Smith, G.T. Norris, A.G. Snyder, J.P. Kolb, et al., The nucleotide sensor ZBP1 and kinase RIPK3 induce the enzyme IRG1 to promote an antiviral metabolic state in neurons, Immunity 50 (1) (2019) 64–76 e4.
[72] B.D. Paul, S.H. Snyder, V.A. Bohr, Signaling by cGAS-STING in neurodegeneration, neuroinflammation, and aging, Trends Neurosci. 44 (2) (2021) 83–96.
[73] C.M. Arbeeny, H. Ling, M.M. Smith, S. O'Brien, S. Wawersik, S.R. Ledbetter, et al., CXA-10, a nitrated fatty acid, is renoprotective in deoxycorticosterone acetate-salt nephropathy, J Pharmacol Exp Ther 369 (3) (2019) 503–510.
[74] Y. Pan, Y. You, L. Sun, Q. Sui, L. Liu, H. Yuan, et al., The STING antagonist H-151 ameliorates psoriasis via suppression of STING/NF-kappaB-mediated inflammation, Br. J. Pharmacol. 178 (24) (2021) 4907–4922.
[75] M.C.C. Canesso, L. Lemos, T.C. Neves, F.M. Marim, T.B.R. Castro, E.S. Veloso, et al., The cytosolic sensor STING is required for intestinal homeostasis and control of inflammation, Mucosal Immunol. 11 (3) (2018) 820–834.
[76] M.K. Skouboe, A. Knudsen, L.S. Reinert, C. Boularan, T. Lioux, E. Perouzel, et al., STING agonists enable antiviral cross-talk between human cells and confer protection against genital herpes in mice, PLoS Pathog. 14 (4) (2018) e1006976.
[77] C.K. Riener, G. Kada, H.J. Gruber, Quick measurement of protein sulfhydryls with Ellman's reagent and with 4,4'-dithiodipyridine, Anal. Bioanal. Chem. 373 (4–5) (2002) 266–276.
[78] K.J. Livak, T.D. Schmittgen, Analysis of relative gene expression data using real-time quantitative PCR and the 2(-Delta Delta C(T)) Method, Methods 25 (4) (2001) 402–408.